An experimental study of the stability of oscillatory-flow bed configurations

by

John McClements Lambie

B.S., M.I.T.
(1983)

SUBMITTED TO THE DEPARTMENT OF
EARTH, ATMOSPHERIC, AND PLANETARY SCIENCES
IN PARTIAL FULFILLMENT OF THE
REQUIREMENTS FOR THE
DEGREE OF

MASTER OF SCIENCE

at the

MASSACHUSETTS INSTITUTE OF TECHNOLOGY

February 1984

Signature of Author_____
Department of Earth, Atmospheric, and Planetary Sciences
February 3, 1984

Certified by_____
John B. Southard
Thesis Supervisor

Accepted by_____
Theodore R. Madden
Chairman, Department Committee

An experimental study of the stability of oscillatory-flow bed configurations

by

John McClements Lambie

Submitted to the Department of Earth, Atmospheric, and Planetary Science
on February 3, 1984 in partial fulfillment
of the requirements for the Degree of
Master of Science in Geology

ABSTRACT

Oscillatory flow over a sediment bed produces characteristic bed configurations over a range of flow conditions. The characterizing variables of the flow, if properly grouped into dimensionless parameters, can be represented in a three-dimensional space that reveals the range of flow conditions necessary for a particular bed phase. The parameters used here are linear in terms of grain size D, maximum orbital velocity U_m, and oscillation period T. Seven bed phases exist in distinct but not necessarily unique regions of the parametric space. The seven bed phases are: no movement, rolling-grain ripples, two-dimensional (2D) vortex ripples, three-dimensional (3D) vortex ripples, reversing-crest ripples, vortex ripples and reversing-crest ripples, and planar bed.

Two series of experimental runs were made with different sand sizes in an oscillatory-flow duct that was tilted about a central pivot by an eccentrically driven connecting rod. The closed duct, 5.88 m long, produced pure oscillatory flow over a 2.44 m long x 0.25 m high x 0.10 m wide test section. Water ran up into overhead storage tanks at either end of the duct where it was heated to 60° C for scaling of the results. External measurements were made of temperature, oscillation period, and orbital diameter. The data show good fit with an empirically derived curve for the threshold of sediment motion in oscillatory flow. Rolling-grain ripples are a transitory bed form for most flow conditions but have their own distinct and unique stability field at small U_m and T for fine sands. 2D vortex ripples, the most common bed form in the range of natural flow conditions, develop in flow with moderate U_m and small to large T. 3D vortex ripples develop at larger U_m and lower T relative to 2D vortex ripples and are stable up to the conditions of planar beds. Reversing-crest ripples occur in higher energy flows than vortex ripples; dimensionless T appears to be the dominant parameter in their formation with a lower boundary value of approximately 7 s. The overlap region between vortex ripples and

reversing-crest ripples is only within the realm of natural flow conditions for very fine sand at large U_m and moderate T. Planar beds occur at a combination of large U_m and large T.

Thesis Supervisor: Dr. John B. Southard

Title: Associate Professor of Geology

The greatest thanks go to John Southard for his inspiration and patience in guiding me through this work. The enthusiasm that he shows in both classroom and personal discussion initiated my interest in the field of sedimentology. The simplifying language,clarity of thought, and the endless energy he has for his students and his work has made it a delight to work with him. Aside from encouraging and helping all through the research endeavor John Southard's greatest contribution to my work was the clarity of speech and thought that he rendered to the text. For this and all that he has aided me in I am deeply indebted.

Ole S. Madsen helped in clarifying my thinking during the formative stages of my thesis. For the time he spent talking with me I thank him heartily.

I am grateful to John Annese who helped immensely in the construction of the apparatus and who took the time to listen. I thank Jim Danna for his astounding ability to solve mechanical problems and for his organization of a student work crew in the Center for Experimental Sedimentology that was always there to help. A debt is owed to Harold (Doc) Edgerton and his assistant Bill for mending the strobe and calibrating it after many years of use in sandy environments.

I thank Judith Stein for her sense of self and her words of criticism and support for me. Her adept handling of the red tape in the early stages of the project kept things moving. I thank: Doug Pfeiffer for his ability to manage the finances of this department and still smile at the people who go overbudget, Debby Gillett Roecker for the comfortable work environment I enjoyed, and William Brace for sustaining a cooperative and excellent scientific group.

My fellow graduate students have made learning lively and interesting during my time here. I thank, Doug Walker for his interest and enthusiasm for my work, Dave Klepacki for his tolerance and his love for geology, and Dayton Marcott for his evenhandednes and patience. I am grateful to Janine Commerford for the mutual support and friendship we have given each other. I thank Roger Kuhnle for his humor and good company. In particular I would like to thank Peter Wilcock for the diverse and constructive conversations we have had in the past few months (I hope that the right team will win).

I thank Marsi Thelin for her love and for her help in finishing this work.

I thank my friends, all of them. They are my greatest asset in coping with this world and I cannot express my gratitude.

I am forever indebted to my parents, Andrew and Margaret for their love, support, teachings, and concern. My family has prodded and nurtured me all through my life and helped me to realize my goals. I can only hope that this work represents them fairly.

INTRODUCTION

Bed configurations under oscillatory flows have been studied for over a century but understanding is still imperfect. The complexity of the physics involved in theoretical consideration of oscillatory flow has limited experimental studies to empirical equations for observed results. The first laboratory studies of oscillatory flow in the 19th century by Hunt (1882) and Darwin (1883) related the bed forms at the fluid-solid interface to the action of surface waves. Later studies by Bagnold (1946), Komar (1974), and Lofquist (1978) attempted to correlate flow parameters to observed bed features using theoretical considerations and empirical observations. In his classic paper, Bagnold (1946) produced oscillatory-flow ripples by moving a sediment tray in a tank of still water. Unfortunately this technique does not produce the same velocity field as a fluid moving over a stationary bed, but Bagnold's theoretical relationship between the orbital excursion of a fluid particle and the spacing of the bed forms remains tenable. Komar and Miller (1973) modified Bagnold's relationship to make it a dimensionless grouping of flow variables. They then found that it had a very good fit with existing laboratory data for which boundary roughness was less than the thickness of the oscillatory boundary layer. Several investigators have produced their own data sets: Manohar (1955), Kennedy and Falcon (1965),

Carstens et al. (1969), and Mogridge and Kamphuis (1972). The results of each are similar but none is a complete data set. The data sets show scatter when plotted together on a single graph; this probably results from differences in experimental arrangement rather than in flow conditions (see Southard, 1982).

The analytical work based on these data sets yielded an agreement in principle amongst the different investigators as to the mechanics controlling certain observed phenomena. In the vortex-ripple stability field a ratio of length scales, the orbital excursion of the fluid divided by the sediment grain size, is observed to bear a linear relationship to the spacing of bed forms. This relationship is function of the size of the vortex cells in oscillatory flow over an unconsolidated boundary. Kennedy and Falcon (1965) recognized from theoretical considerations that in the absence of a drift velocity the relationship between ripple spacing and orbital excursion of the fluid is a function of the period of oscillation. Thus the same orbital excursion at different periods of oscillation will produce distinct and different bed forms with their own characteristic spacing.

Lofquist (1978) divided the range of oscillatory-flow conditions into regions in which different flow parameters control the bed configuration. The higher-energy flows depend on a term in which viscosity is an important variable controlling the dissipation of flow energy during a half

cycle. The lower-energy flows depend on the orbital excursion of a fluid particle. The analysis is sound but the relationships obtained provide little insight into the phenomena of oscillatory-flow bed forms.

Theoretical work on oscillatory-flow bed forms has been more extensive in recent decades. Bagnold (1946) derived the first theoretical relationship for the initiation of sediment movement under an oscillatory boundary layer. Yalin and Russell (1963) developed arguments for considering oscillatory-flow environments in terms of a few dimensionless groupings instead of numerous flow variables by applying Buckingham's Theorem. They then developed a model in which only three dimensionless groupings are important to characterize the flow regime for any particular set of conditions. Komar and Miller (1974) developed an empirical relationship for initiation of sediment movement from theoretical work on the boundary shear stress at the sediment bed. Clifton (1976) presented the first model for determining bed-form stability from the flow parameters he devised. Clifton's conceptual model attempts to predict the general nature of ancient sedimentary conditions that produced observed bed-form sequences.

The purpose of the present study was threefold. The first objective was to produce a self-consistent set of data spanning a wide range of sedimentological conditions, eliminating the problem of differing experimental arrangements. The second was to address certain questions

on bed-form stability. Lastly the study applies a synthesis technique to a large collection of existing oscillatory-flow data and interprets the result. Some of the questions addressed in the second phase of this study are: (1) Do rolling-grain ripples grow into vortex ripples even at the smallest velocities for which ripples develop? (2) Are stable vortex ripples possible at maximum orbital velocities U_m below the threshold of movement? (3) What is the nature of the transition from vortex ripples to nonvortex ripples with increasing U_m and period T? (4) What is the relationship between two-dimensional (2D) and three-dimensional (3D) vortex ripples?

The synthesis of data from other experiments relies on a dimensional analysis in which dynamic similitude is used, scaling all properties of the flow and bed according to a Reynolds-Froude model. The result is a viscosity scaling of all the data to a parametric space. For the purpose of this study a set temperature of 10°C was taken and all data scaled to the appropriate viscosity and density. Southard, Boguchwal, and Romea (1980) first established the validity of scaling data for open-channel flume experiments by performing dynamically similar runs with fluids of different viscosity. Since no data exist to support this type of argument for oscillatory-flow experiments, two experimental runs were made in which experimental conditions were matched as closely as possible to those of a previous run. This produced two pairs of runs in which flow

parameters were matched. The resulting correlation of bed forms is very good and arguably validates the use of the data synthesis in the subsequent analysis.

EXPERIMENTS

General

The task of producing a good analogy to the bottom oscillatory flow produced by propagation of shallow-water gravity waves in a laboratory tank is not a simple one. Different techniques have been used in the various studies done on oscillatory-flow phenomena. Darwin (1883) used a novel experimental method in which a cylindrical vessel filled with sand and water was oscillated back and forth around a vertical axis to produce bed forms. Bagnold (1946) and Manohar (1955) both used submerged sediment trays shifting back and forth in simple harmonic motion. There are at least three problems with this: the velocity profile above the bed is inverted, accelerations of particles are not taken into account, and the pressure surge associated with a passing wave is absent. The most commonly used experimental method for producing oscillatory flow is a long tank with a sloping model beach at one end and a wave generator driven by an eccentric drive wheel at the other. This makes waves of a given amplitude and period that travel the length of the tank and expend themselves on the beach. The resulting near-bottom flow field is a very good analogy to that produced by surface gravity waves in an open water natural environment. Observations are made in the middle of the tank away from both the generator and the beach. There are two major limitations to this arrangement. First, the range in oscillation period is small because inciting longer

period oscillations requires a large excursion of the generator and a very long tank to accommodate the wavelength of oscillation. Second, the reflection of waves off the beach sets up standing waves. This is avoidable by tuning the apparatus to eliminate standing waves but it further limits the available experimental conditions to be tested.

Carstens et al. (1969) first oscillated water in a U-tube oscillatory-flow duct. The oscillation was induced by a harmonic variation in the pressure gradient over each end of the system. The water oscillated at a more or less constant resonant period of 3.5 s while the magnitude of oscillation was varied. The limitation to a single resonant period seriously restricts the usefulness of this arrangement. Variation in resonant period could be achieved by making the duct length adjustable.

The experimental arrangement used in the present study is similar in principle to that of Carstens et al. (1969). The variables important in a sedimentological study of bed forms, along with the principal objective of collecting a large uniform data set, dictated the choice of apparatus. A closed oscillatory-flow duct produces a linear water motion over a sand bed. Oscillatory flow was produced in a tilting duct driven by an eccentrically driven connecting rod and gearmotor. By tilting the duct see-saw fashion a pressure head is developed at one end equal to twice the amplitude of the motion of the duct. This produces a velocity surge toward one end which is slowed to a stop by the subsequent

increase in pressure head from tilting of the duct. A distinct phase lag then exists between the motion of the fluid and that of the duct. The motion of the fluid is symmetrical with respect to any point on the sediment bed. The driving of the fluid means that a wide range of periods and velocities can be tested. The natural resonance of the apparatus produces larger velocities at the resonant period but does not upset the experimental analog. A variable-speed gearmotor in combination with an eccentric drive disk with a range of orbital radii allows a full range of flow conditions to be created.

Consideration of two important flow variables, maximum orbital velocity U_m and oscillation period T, led to the construction of a device in which velocity was measurable in two different ways. The orbital diameter 2a of the water motion was measured and taken to represent U_m through the relation

$$U_m = \frac{2\pi a}{T} \tag{1}$$

The second method was to measure the variation in water level in the overhead tanks and determine the average velocity $\bar{U}$ and calculate U_m from the sinusoidal relationship:

$$U_m = \frac{\pi \bar{U}}{2} \tag{2}$$

The experimental program was worked out with ease of measurement in mind for the most important variables in the problem.

From previous work a distinct range of velocities and periods appeared most appropriate in terms of accessibility and simulation of a real flow environment. Ocean waves range in period from 1-3 s to above 20 s under severe storm conditions. The bottom velocities associated with these periods have a large range from below 0.1 m/s to above 2 m/s. A realistic laboratory apparatus could not produce the highest periods and/or velocities. Since much data exist for the smallest periods ($T \leq 2.5$ s) and little above 7 s the equipment used was designed to produce oscillations with long period as well as short and intermediate period. The size of the duct was limited by weight considerations. The limit in ripple spacing was eliminated by using a duct that was long relative to ripple spacing. Lofquist (1978) noted that an integral number of ripple spacings always appeared in his experiments; the end effects responsible for this phenomenon were reduced by increasing the length of the test section. The anticipated vortex ripples required a height clearance of 10-15 cm. Thus the height was kept as small as possible and scaling was exploited as far as reason and rigour would allow.

Once all the above were defined a mathematical analysis of the stresses, energy, work-load, heat loss, etc. was performed. The resulting figures demonstrated that an experimental apparatus could be constructed that was reasonable in cost and size but most importantly could produce a good analogy to an oscillatory-flow environment

without producing a significant gravity slope.

Apparatus

The experiments were made in a simple U-tube oscillatory-flow duct. See-saw tilting of the duct incited oscillatory motion of the fluid over the sediment bed by driving water between two overhead storage tanks connected to the ends of the duct. The duct was 4.88 m long, 0.10 m wide, and 0.25 m high in inside dimensions. A section of clear Plexiglas 2.44 m long allowed viewing of experimental results in the sediment bed. The duct rested upon a rigid beam constructed of plywood and steel. A series of cross-ties provided the top surface for the duct to rest upon. These cross-ties were held on threaded rods with nuts allowing for levelling of the duct after placement (Figure 1). The central pivot was a sturdy triangular base with bearing blocks on the top. The underside of the beam was fitted with similar bearing blocks, and a steel shaft served as the axle.

An eccentric connecting rod powered by a variable-speed gearmotor tilted the duct and beam assembly about the central pivot. Two reduction shafts external to the motor provided a further reduction in the speed of the drive disk. The 1/2 hp gearmotor had a speed range at the output shaft of 18-108 rpm. The eccentric connecting rod was a piece of 2x4 lumber 0.46 m long with two solid bronze bearings press fitted into holes at either end. The angle of tilt of the

duct was varied by repositioning a hand-machined connecting pin on the drive disk. The drive disk was made of a 1"(2.54 cm) thick piece of aluminum plate cut to a circle 35 cm in diameter. A spiraling array of holes was drilled in the aluminum plate at 1.25 cm intervals beginning at a radius of 2.5 cm and ending at 16.5 cm. The change in orbital radius altered the amplitude of motion of the duct. The connecting pin was inserted into one of the bronze bearings and acted as a bearing surface itself. The other bronze bearing fitted on a piece of shafting connected to the underside of the beam. The drive assembly produced periods of oscillation from 2.3 s up to 14.6 s (unscaled).

The overhead storage tanks at either end of the duct were made of plywood and fastened to the top of the duct using a neoprene rubber gasket with grease for a seal. The tanks were rectangular boxes 61 cm x 61 cm x 46 cm. The passage between duct and tank was a rectangular opening 5 cm x 40 cm with curved edges to reduce turbulence in the flow. The cross-sectional area of the passage was approximately equal to the cross-section of the duct through which water passed (10 cm wide x 20 cm high). At either end flow-control pieces were inserted to smoothly turn the flow from horizontal to vertical into the tank and vice versa (Figure 1). False bottoms 5 cm high were installed to stabilize the flow and develop the boundary layer before the flow reached the test section. The false bottoms effectively extended to the edges of the Plexiglas windows,

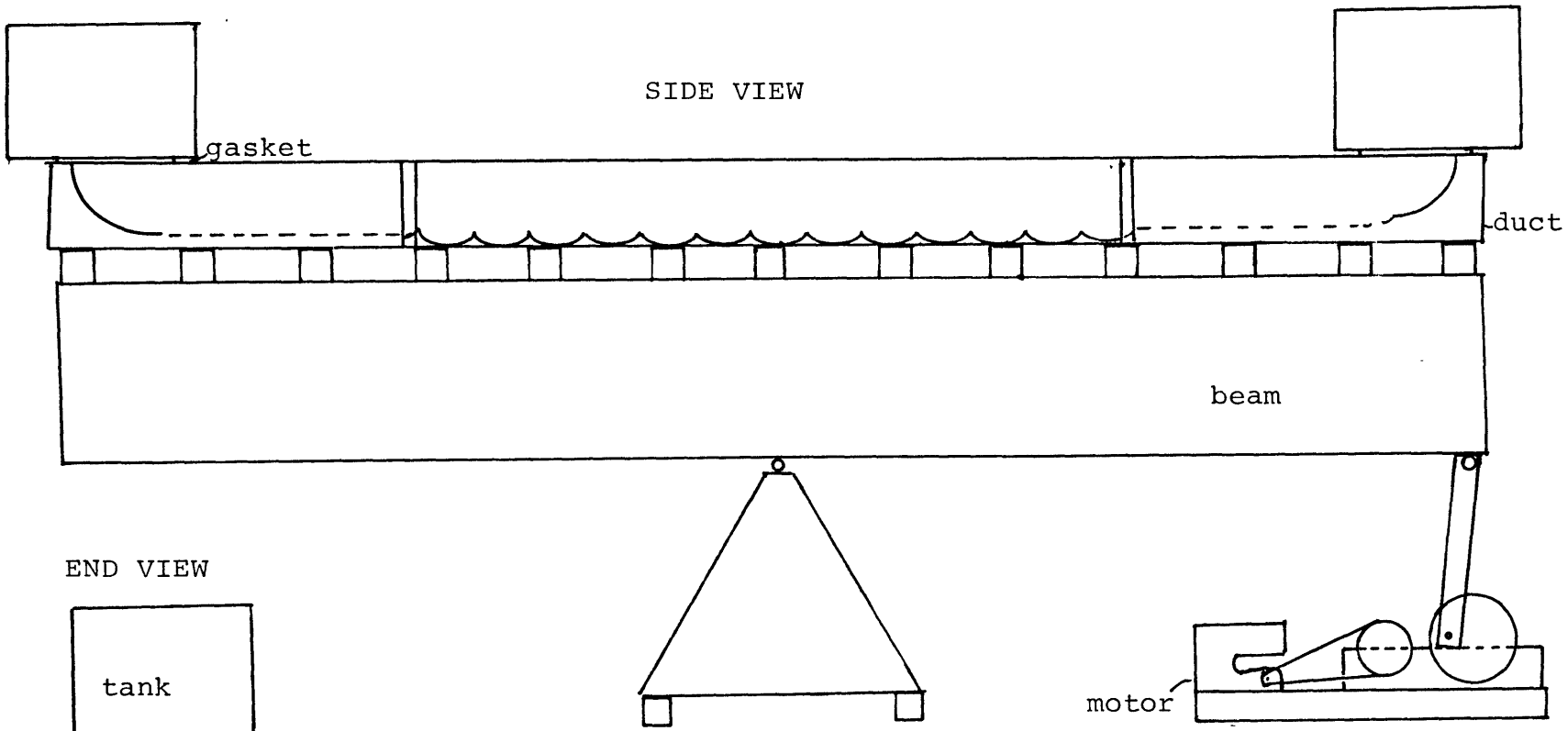

Figure 1: Experimental apparatus.

leaving a section 2.44 m long for experimentation. The ends of the duct were designed to be removable, allowing access to the sediment bed when needed. These end pieces were held to a large wooden flange at the ends of the duct by bolts, and a watertight seal was made with neoprene rubber for a gasket and a heavy application of lubricating grease.

Photography

Photographic records were made both during and after runs. A 35 mm SLR camera was used to record the bed configuration at the conclusion of a run. Run data were posted on the wall and included in each frame. Time-lapse sequences were produced using a Bolex H16 Reflex camera. The camera was triggered by a mounted solenoid connected to a movie timer set to trip every 5 s. Bed growth could then be observed at leisure, and long-term events or details were recorded. The camera rested on a long metal bar connected to the moving duct. This arrangement eliminated any relative motion between the duct and the camera. A scale was kept in the field of view along with a chart of relevant run data. Backlighting with an array of tungsten lamps allowed a reasonable depth of field in the filming.

Attempts were made to measure the velocity profile by taking closely spaced exposures of a half-cycle of the fluid motion, but with only partial success. This can be done either with high-speed photography or with an open camera shutter and a high-speed strobe. The latter was employed to

illuminate neutrally buoyant particles in the flow. A Polaroid Instamatic camera with a Buschnell lens was used to obtain open shutter exposures in a dark room with only the strobe for light. The strobe used was a Type 1538A General Radio Strobotac. Back light was restricted in the laboratory by using black opaque shower curtains on the windows. Photos were taken at night to increase the chances of success. Unfortunately the particles were two small to appear on the film without overexposing it. A second method using the strobe light on water-filled ping-pong balls was also unsuccessful because they continually bounced off the top and side walls of the tank, distorting their motion and reducing their visibility. A third technique using the Bolex camera for high-speed filming of suspended material in the flow did capture the velocity pattern over the flow cycle but requires a good 16 mm film projector in order to obtain the actual velocity profile. Such a frame-by-frame projector was not available in time for inclusion of the data in this report.

Small neutrally buoyant particles provided flow visualization for both photography and velocity measurements. The particles were simple to make and extremely reflective. A mixture of candle wax and TiO_2 was melted and homogenized. The mix was then placed in an old-fashioned garden bug sprayer and reheated to liquid form. Pumping the mix through the sprayer atomized the fluid into small beads with varying TiO_2 content. A bucket

of water served as the catchment for the atomizing process. The floating portion was removed and the neutrally buoyant fraction decanted. This provided small white particles for the strobe technique. Measurements of the orbital diameter 2a were made using these same neutrally buoyant particles.

Experimental Techniques

Runs were made with hot water to reduce the viscosity and provide scale modelling of the flow environment reproduced in the laboratory. Hot water was pumped into the duct through the overhead tanks at an average temperature of 45° C. Two self-contained 1150 W immersion heaters placed in over the side of the storage tanks heated the water to above 60° C. Once the water temperature reached 60° C one heater was switched off and the system allowed to thermally equilibrate. In addition to the heaters, closed-cell polystyrene foam insulation was fixed to all sides of the flume and tanks except for the endplates and underside of the duct. Also the Plexiglas sections in the center of the duct were left clear for viewing and filming of events in the duct. The open surface in the storage tanks was fitted with pieces of foam insulation that floated on the water surface. The calculated heat loss for the system with 1" (2.54 cm) foam insulation was roughly 1300 W at 60° C. The conservative estimate of the insulation rating on the wood surfaces explains the higher temperatures obtained (Table 1). The effects of turbulence on heat conduction were also

clearly observed in the variation of temperature with flow energy. Temperature measurements were easily obtained by inserting a long mercury thermometer down through the storage tanks into the flow in the duct and reading to ±0.1° C.

Two different sand sizes were used. These size fractions were obtained by wet-sieving between two closely spaced sieve sizes. The modal size of each fraction was regarded as the characteristic sediment size of that fraction. The coarser sand had a modal size of 0.15 mm and the finer sand had a modal size of 0.09 mm. Both were derived from quartz sand from the Ottawa Silica Co. and small amounts of remnant sediments in the Center for Experimental Sedimentology at MIT. The sediment-bed thickness was designed to be 5 cm in average, but for some runs this was increased to prevent scouring to the floor of the duct. Access to the bed after each run was restricted by the experimental configuration. Therefore to flatten the bed, the duct was drained and a shallow depth of water left behind to flow back and forth at supercritical velocities to flatten the bed. This was not done in all runs since in some runs hysteresis was to be studied between different flow conditions and their associated bed forms. When necessary both ends of the duct were removed along with the flow-control pieces to allow removal of the sediment.

Runs were usually initiated with a planar sediment bed. Once the water reached its equilibrium temperature, U_m and T

were measured. T could be measured externally from the motion of a fluid particle or a notch on the drive wheel; agreement between the two was universal. At this point the nature of the initial bed configuration was noted, and in some cases the bed forms were measured and recorded. Time-lapse photography began at this point if it was to be done (only ten runs were filmed). The run was then left to reach equilibrium; this took 4-6 hr in high-velocity flows and up to 48 hr at the lowest velocities for which sediment actually moved. At the end of a run U_m and T were checked and recorded again. The duct was stopped and the bed forms were photographed. If regular in size and spacing the bed forms were measured, but otherwise they were left to qualitative descriptions. Qualitative observations of bed-form development were made during runs. Stratification in the sand was largely ignored since it was not part of the experimental program. However, some interesting features of the stratification were noted during runs and are presented in the next section.

Between runs the water was removed using siphon hoses. The oscillation period was adjusted both by changing the internal gearing of the gearmotor and by rearranging the external gear ratio of the two reduction shafts. The orbital path of the connecting rod together with the oscillation period directly controlled U_m of a run. The tilt of the duct was changed from run to run to produce different values of U_m. Runs were usually made in a

sequence of steadily increasing or decreasing U_m at constant T. The apparatus was cleaned between runs; in exceptional cases the end plates were removed to do this.

RESULTS

Series of Runs

The 34 runs with the coarser sand yielded relatively uniform results. The variables D, U_m, and T appear in Table 1 along with ripple spacing λ, ripple height h, and water temperature. The bed configuration at the end of each run is also listed in Table 1. The geometry of the bed and nature of the flow over the bed served as criteria for classifying the bed phase. If flow over the bed contained distinct vortex cells, then the bed-phase name contains the word vortex or some such desriptor.

The classification used for both sands is taken from terminology and descriptions of bed forms in previous investigations. The following is a compilation of the names used in describing oscillatory-flow features. The term no movement (NM) refers to conditions below that of incipient grain movement. Rolling-grain ripples (RGR), first described by Bagnold (1946), appear after the movement of the first few grains, and align themselves roughly perpendicular to the flow. The most frequently observed bed form was two-dimensional (2D) vortex ripples . In such cases the bed forms have a distinct and uniform spacing and height, with horizontal ripple crests that are perpendicular to the flow direction. The shoulders of 2D vortex ripples are typically concave upwards. At higher velocities the ripples become less regular. The bed configuration in these higher energy flows had ripple crests that bifurcate and

anastomose into other ripple crests across the flow direction. The flow contains distinct vortex cells that have no regular pattern but are constantly changing the bed geometry and being altered by the bed surface. These irregular-vortex bed forms are called three-dimensional (3D) vortex ripples. Near the transition from a 2D to a 3D bed configuration a characteristic ripple spacing and height for the bed forms existed and was recorded.

At combinations of high velocities and long periods the bed forms had no short-term stability. During each half cycle of the flow the bed forms suffered erosion and the sediment was transported as both bed load and suspended load and then redeposited during flow deceleration. Therefore the ripples had instantaneous unidirectional character with a lee and a stoss side. The name assigned to these ripples by Inman (1957), reversing-crest ripples (RC), will be used in this report. The ripple spacing relative to the 2a of the flow was small and the ripple height was 2 cm at most. In the coarser sand reversing-crest ripples were often superimposed on large vortex ripples of both 2D and 3D character.

The last commonly observed bed form in the first series of runs was a sequence of regular and asymmetrical unidirectional-current ripples that appeared on the shoulders of large 2D vortex ripples. The lee side lies crestward of the stoss side and they are usually present on both sides of a vortex-ripple trough. The size of the

ripples increased to a maximum near the 2D vortex-ripple crest. Upper-planar-bed conditions (PB) at high Um and T produce no ripples, only planar laminae.

The 36 runs in the second series, with the very fine sand (D= 0.09 mm), yielded a greater diversity of bed forms and a larger number of bed phases. The variables measured are listed in dimensional form in Table 2 along with the bed phase. The seven kinds of bed phases described in the following (no movement, rolling-grain ripples, 2D vortex ripples, 3D vortex ripples, reversing-crest ripples, reversing-crest ripples plus vortex ripples, and upper planar) were all seen in different runs using the finer sediment size. There were no differences in experimental procedure between the two series of runs, but more extreme conditions of U_m and T were modelled with the finer sediment. The high-velocity conditions for the coarse sediment produced bed forms with a spacing and height that the apparatus could not model. Such runs were not recorded in the data set, excepting two whose bed phase seemed 2D vortex in style. Sediment movement occurred at lower values of U_m and T. Only one run was made in which no movement occurred. This was at scaled U_m, U_m^*=0.098 m/s and scaled T, T^*= 4.1 s. The slightest sediment movement resulted in development of 2D vortex ripples from an initial bed of rolling-grain ripples. Rolling-grain ripples were not seen on the sediment bed at the end of any run.

The transition between 2D and 3D vortex ripples was

observed at several different periods in order to determine the combination of conditions that define the boundary between the two bed phases. Runs 20 through 26 in the coarser sand, made to test the stability of 2D vortex ripples down through the no-movement boundary, showed 2D vortex ripples present below the no-movement threshold. Preferential erosion of the 2D vortex ripple crests occurred at slower flows, but the ripple shape did not degenerate before sediment motion ceased. Growth of rolling-grain ripples into vortex ripples from a plane bed at these low-energy conditions took from 24 to 48 hr (unscaled).

Reversing-crest ripples were first seen at high velocities in the finer sand at $U_m^* = 0.5$ m/s and $T^* \doteq 8.5$ s. Reversing-crest ripples formed in flows up to 20 s in period in the finer sand.

In general the two series of experiments produced similar results. There were fewer kinds of stable bed form in the coarser-sand runs. The style of bed-form development was similar in the two series. Finite elements in the sediment surface topography disturbed the flow over the bed for both series. With this similarity in flow kinematics one would expect to observe similar bed configurations.

Observations of Bed Forms

The few no-movement runs made were not completely straightforward. In the coarser sand, several runs produced no significant bed forms and yet a very small

percentage of grains were set in motion at the start of these runs. By the time these runs were terminated all sediment motion had ceased. In two of the three runs small bed forms resembling rolling-grain ripples appeared and then ceased to move or to gain any new sediment. The minor grain movement at the start of these runs ceased by the time the whole system reached its equilibrium temperature of roughly 60° C. The lack of growth and movement in these runs placed them in the region of no-movement flow conditions.

Rolling-grain ripples were seen at the start of many of the runs. In most runs they were transitory, disappearing soon after the run began. Usually they gave way to vortex ripples, but in some cases they grew into reversing-crest ripples. In the runs in which rolling-grain ripples were only a transitory bed form, the style of flow circulation changed drastically as the ripples grew and moved on the sediment bed. No runs in the finer sand produced rolling-grain ripples as the stable bed form. In all runs with the finer sand in which rolling-grain ripples appeared, they grew into some other bed form. The threshold of sediment motion in the finer sand was reached suddenly when increasing the velocity of the flow from run to run. The two runs that produced rolling-grain ripples in the coarser sand were at lower flow velocities than two of those which produced no eventual bed forms. This result appears anomalous at first glance and will be discussed later.

The rolling-grain ripples observed were like those

described by Bagnold. They aligned themselves roughly perpendicular to the flow but were not straight-crested. Each half cycle of motion moved a high percentage of the sediment in a particular ripple. Sediment transport diminished with time. However, rolling-grain ripples grew with time, and in most runs they moved relative to one another and merged to form larger vortex ripples.

Two-dimensional vortex ripples were the most common bed form. The development of 2D vortex ripples was always preceded by rolling-grain ripples. Rolling-grain ripples appeared after the first few oscillation cycles; the spacing and height were a few centimeters and a few millimeters, respectively. Ripple spacing and height grew with time, disturbing the flow. A symmetrical ripple profile was characteristic of 2D vortex ripples. The spacing-to-height ratio λ/h was roughly 6 (Tables 1 and 2). Spacing of 2D vortex ripples ranged from 6.6 to 110 cm (unscaled). The vortex cells in the flow associated with 2D vortex ripples have horizontal rotational axes and are highly symmetrical. The concave shoulders of the vortex ripples were typically smooth and curviplanar. A scour pocket occasionally developed in the center of the ripple shoulder about halfway from trough to crest. Trough profiles also grew, with some showing very steep sides and a well at the lowest point. Alternatively some troughs were relatively long and flat with little scour.

In several runs, bed forms with a vortex-ripple

geometry formed in the center of the vortex-ripple troughs. These trough ripples are denoted as TR in the tables. Their height was less than that of the 2D vortex ripples and the internal laminae were different in style. The 2D vortex ripples contained laminae on both shoulders. The center point of the ripple under the crest resembled a shuffled deck of playing cards before sorting. Interfingering layers from either side crossed the center point under the crest.

In certain runs the laminae in the 2D vortex ripples showed the history of ripple growth. The laminae in the vortex ripples showed progressive aggradation away from a neutral point in the sediment bed. The ripple under the neutral point showed laminae as previously described, but to either side the vortex ripples contained uniformly sloping laminae with opposite slopes.

In most runs with 2D vortex ripples, both bed load and suspended load were abundant. In runs with bed load predominant, size fractionation developed between crest and trough; the coarser grains were deposited near the crest and the finer grains settled in the troughs. This was easily observed because of dark grains that formed lines on the bed surface a well-defined distance from the ripple crest demarcating the two regions.

3D vortex ripples were produced by vortex-dominated flow, as the name implies. As with 2D vortex ripples, the bed forms first produced from a plane bed were rolling-grain ripples with no regular spacing. Once ripples had

developed, the vortex cells continued to transport sediment to them in a positive-feedback loop. But unlike the 2D vortex ripples, the 3D vortex ripples did not stabilize with a particular geometry; instead the bed forms continually changed position and shape. Ripple crests were irregular in height and plan pattern, and showed no preferential orientation with respect to the flow. Pockets appeared on either side of transverse ripple crests. There was a great deal of variability in 3D bed shape, but no quantitative measurement were made.

Three different styles of bed geometry were clearly seen in the 3D vortex ripples. The first was a simple breakdown of stable 2D vortex ripples to a bed consisting of semi-regular ripples with nonhorizontal crests but definable spacing and height. The second was a pattern of continuous ripple crests that curved across the flow direction; they too had a definable spacing and height. The third and most common style was a random pattern of local highs and lows with discontinuous crests. This last style was associated with flows in which vortex eddies with both horizontal and vertical axes appeared. This produced local scours in the bed and vertical vortex-eddies in the flow. No characteristic stratification pattern was seen in any of the 3D vortex ripple types; their mobility precluded such observation in this investigation.

The next most common bed form in this study after vortex ripples was reversing-crest (RC) ripples.

Reversing-crest ripples, formed at larger T and Um, are different from vortex ripples in that the flow contains no observable circulation cells. The flow appears to be laminar or smooth turbulent and more or less linear throughout an oscillatory cycle. Reversing-crest ripples were observed only in the finer sand, even though the same flow conditions were used in the runs with the coarser sand. The development of reversing-crest ripples preceded any other ripple type that developed in the same run. They appeared immediately on the sediment bed. However, they grew in height and spacing with time. The orientation of lee and stoss sides reversed during each half cycle of the flow. Thus the sedimentary record produced by the flow environment for reversing-crest ripples shows planar laminae.

Reversing-crest ripples accompanied vortex ripples in five of the eight runs in which they formed. In these runs the reversing-crest ripples always developed first. In some of these runs reversing-crest ripples were seen only on the shoulders of the ripples and not in the troughs. Reversing-crest ripples were more asymmetrical when developed on vortex-ripple shoulders but still changed orientation during each cycle. The highest energy flow conditions which produced reversing-crest ripples were U_m= 0.575 m/s and T= 19.4 s. No other bed forms could be modelled at this large a period. Higher velocities yielded planar beds or enormous bed forms.

Reversing-crest ripples formed when suspended load appeared all throughout the observed near-bottom boundary layer of the fluid. This boundary layer extended 5-10 cm above the sediment surface and was virtually opaque due to the suspended load.

Unidirectional-current ripples were an interseting bed feature of longer period runs. These ripples formed in the troughs and on the shoulders of 2D and 3D vortex ripples. The side profile of these bed forms was asymmetrical with a clear-cut lee and stoss slope. The lee slope was always toward the ripple crest. Spacing and height of these ripples increased from the lowest point in the trough toward the crest of a vortex ripple, producing a unique pattern of sediment laminae. The foreset laminae varied from 0° to 10° dip in either direction due to the combination of vortex and unidirectional-ripple geometries.

The term unidirectional applied to these bed forms is clearly genetic but the observed flow conditions warrant its use. The sediment bed experiences different flow conditions spatially under oscillatory flow. Vortex cells are geometrically confined by local topography. The flow separation near the crest of a vortex ripple creates a velocity shadow on the downcurrent side. The resultant recirculation eddy impinges on the sediment bed with an upcurrent velocity before the flow reverses. Thus the resultant velocity vector is stop-start unidirectional rather than oscillatory. This mechanical scheme produces an

inherent timing relation between vortex ripples and unidirectional ripples. The vortex ripples grow from an initially planar bed, and after reaching relatively large size they begin to shadow the downcurrent side during each half cycle. This promotes growth of unidirectional ripples on the shoulders. The unidirectional ripples perturb the vortex cells of the 2D/3D vortex ripples as well as producing their own small lee-side vortices. The observed effect on the vortex ripples was steepening of the flanks and an increase in λ. Ripple laminae showed three distinct growth phases as a result: symmetrical-oscillatory, pseudo-horizontal foreset growth, and asymmetrical-oscillatory plus foreset laminae. The unidirectional features described were seen in conditions of $U_m^* = 0.5$ m/s and $T^* \geq 7.5$ s.

The last observed bed phase is that of upper-planar-bed flow (PB). Clearly, from the name, no bed forms were produced under the highest velocities and periods tested. A large quantity of sediment moved during each half cycle of oscillation but was deposited rapidly, leaving no flow-controlled bed features. Much sediment remained in suspension while the flow decelerated and stopped. Bed load shifted from one end of the tank to the other, and the resultant strata are thin laminae. The smallest period at which planar laminae were seen was $T^* = 8.0$ s and $U_m^* = 0.975$ m/s. Although they moved a great deal of sediment, lower velocities at longer periods produced no bed forms. The flow

above the bed was like that of reversing-crest environments, with no small-scale or large-scale vortex cells visible. Small-scale turbulence predominated in the flow, making velocity measurements based on 2a less certain than the method using mean fluid-level change in the head tanks.

The results of the time-lapse photography highlighted several notable features of the observed bed forms. Filming of runs showed that vortex ripples do not migrate once they have fully developed. They migrate only while they are growing and altering the flow. They did not travel any distance; they moved relative to one another to form a new ripple spacing and geometry. The lack of migration seen in footage of 3 to 4 hour time spans confirmed the symmetry of the flow environment induced by the experimental equipment.

The results of Run 18 in the finer sand appear on film in two short segments--one at the beginning, which shows reversing-crest ripples, and one after twelve hours, which shows vortex ripples. The RC sequence shows no distinct growth of ripples on the bed or vortex cells in the flow. The reversing-crest ripples switch back and forth, leaving a linear set of laminae. The latter film sequence shows a trough-to-crest migration and growth of unidirectional ripples on the back of the vortex ripples.

The 3D vortex ripples filmed showed no systematic development or stable geometry. The growth of flow eddies visibly altered the bed forms, and the change in bed configuration was recorded in the time-lapse sequences.

Material was deposited at the edges of visible flow eddies, and material was eroded by the strong linear currents of the oscillatory flow. Both mechanisms eroded and deposited material, but the former showed a less spatially regular pattern of sediment deposition, as seen in the time-lapse sequences. 3D vortex ripples migrate, split in two, grow, and disappear in response to flow above the bed.

Suspended load was universal in flow over 3D vortex ripples. This simplified identification of vortices. Vertical cells developed that locally increased the height of the layer containing suspended load. Troughs or pockets in the bed formed under such cells. The mechanics of vertical cells are not seen in the time-lapse sequences--only the gradual change in the pattern of sediment transport caused by their presence. 3D vortex ripples show no distinctive stratification pattern in time-lapse photos. In summary, 3D vortex ripples migrate, never reach dynamic equilibrium with the flow, and show no regular behavior or stratification.

Test of Scale Modelling

Two sets of flow conditions were used to test the validity of scale modelling of the experimental results. The conditions were fixed by matching the two sediment grain sizes used, via the viscosity dependence of the parameters for oscillatory flow. Once grain sizes were matched, the U_m and T conditions for each run were calculated to fall within

the range of accessible conditions for the duct. The first runs were made with cold (room-temperature) water using the 0.15 mm sand. The velocities and periods are listed in Table 1. Two runs were made with cold water at the different flow conditions. The next runs were made using the 0.09 mm sand. Two runs with 65° C water were made at the flow conditions given in Table 2. The matching was calculated prior to the runs to assure that the values listed in Tables 3 and 4 were as close to each other as possible.

Both hot-water and cold-water test runs resulted in similar bed forms. The first run in cold water produced 2D vortex ripples with small ripples in the troughs. These smaller trough ripples were stable in time and space. Likewise, the hot run produced 2D vortex ripples with smaller trough ripples. The dimensionless spacings λ^* and heights h^* are tabulated in Tables 3 and 4. The values of λ^* are 36.40 cm and 32.2 cm for hot and cold runs, respectively. For the first scale test, the corresponding values of h^* are 4.9 cm and 4.3 cm.

For the second pair of runs, a lower velocity and smaller period were used. The anticipated result was 2D vortex ripples. This is precisely what was seen. An interesting observation was that ripple-crest height varied laterally across the flow in both cold and hot runs at the same hydrodynamic conditions. The values of λ^* are 21.3 cm and 21.6 cm for cold-water and hot-water runs, respectively,

and the corresponding values of h^* are 3.4 cm and 3.7 cm. Thus, with flow variables matched through the scale modelling, we see that the bed variables and bed configuration also match.

Velocity Measurements

The two methods for velocity measurement agree in result. The measurement of 2a was extremely simple. After neutrally buoyant particles were inserted into the flow, their path above the sediment bed could be measured. Measurements made over many oscillations, up to 20 or 30 cycles, showed very good agreement in both low-velocity and high-velocity flows. The position of a particle in suspension was marked on the Plexiglas window at either end of its oscillation path. These marks were then measured and recorded. Averaging over many oscillation cycles improved accuracy.

A machined metal rule, permanently emplaced on the inside edge of one storage tank, allowed measurement of the amplitude of rise and fall of water level in the head tanks. Its position near the inside edge avoided the surface disruption caused by the flow jetting up at the outside edge of the tanks. The volume rate of flow was calculated from the cross-sectional area of the storage tank. The tabulated bed-form height at each 2 cm interval was summed and averaged,

$$\bar{A} = \frac{\sum_{n=1}^{x} A_n}{X} \qquad (3)$$

Then the cross-sectional area of the duct was obtained from Area= (Duct height -A) x width. 2a was then calculated from the equations:

$$Q = \frac{(\text{Headtank excursion} - 2L\sin\theta) \times W \times L}{1/2\ T(\text{sec})} \tag{5}$$

$$2a = \frac{Q \times T(\text{sec})}{2\ (\text{Duct height} - \bar{A}) \times \text{width}} \tag{6}$$

The average velocity for the flow is then:

$$\bar{U} = \frac{2a}{1/2\ T(\text{sec})} \tag{7}$$

The orbital excursion for two runs in the coarser sand showed nearly perfect agreement between the two measurement techniques. In Run 8, 2a measured directly from flow visualization was 38.5 cm, and 2a calculated from the water level in the head tank was 38.3 cm. For a longer period run, Run 30, 2a was 168.1 cm and 170.7 cm, respectively.

DISCUSSION

Data Synthesis

Given a knowledge of the important variables, the number of dimensionless parameters needed to describe the two-phase motion at the sediment-fluid interface can be established by dimensional analysis. Sufficiently strong motion of fluid above a cohesionless bed of sediment produces characteristic topographic patterns in the sediment bed, and any variable associated with these bed forms, like the spacing, depends on the important variables in the problem. If P is such a variable then it may be described as a function of seven independent characterizing variables in the system: fluid density ρ, fluid viscosity μ, orbital velocity maximum U_m, period T, grain size D, sediment density ρ_s, and specific weight γ'. The first six variables in the analysis are understandably present since they are properties of the system. Specific weight relates the relative forces on the particle to its resistance to movement. It should be noted that gravity is an important variable in the problem of oscillatory flow under free-surface gravity waves due to free-surface effects and would have to explicitly stated for analysis of such an environment. Thus:

$$P = f_p\ (\rho,\ \mu,\ U_m,\ T,\ D,\ \rho_s,\ \gamma') \tag{8}$$

Dimensional analysis yields:

$$\pi_p = \Phi_p \left[\left(\frac{\rho\gamma'}{\mu^2}\right)^{\frac{1}{3}} D,\ \left(\frac{\rho^2}{\mu\gamma'}\right)^{\frac{1}{3}} U_m,\ \left(\frac{\gamma'^2}{\rho\mu}\right)^{\frac{1}{3}} T,\ \frac{\rho_s}{\rho} \right] \tag{9}$$

where $\gamma' = (\rho_s - \rho)g$

It should be noted that the orbital excursion of a fluid particle, 2a, bears a linear relationship to U_m and T as seen in equation (1). Therefore only two of these three variables are needed in the analysis.

The first three dimensionless parameters listed are extremely useful because of their linearity with respect to D, U_m, and T. These are three of the most important and easily measured variables in oscillatory-flow environments. The ratio ρ_s/ρ is considered in the data synthesis to be a fixed parameter since natural sediment density is close to the density of quartz in all but a few cases and the density of water varies little over an enormous temperature range. In the runs made in this study, quartz sand was used to fix this parameter. All the data from other investigations that have been analyzed in this study were obtained from runs using quartz sand.

The assumptions made in this analysis are few and involve only simple functions. The form of the waves is assumed to have a certain definite form and the resultant U_m is in the x-direction along the bed surface. Two assumptions about the bed material simplify the analysis: the shape of the sediment particles and the shape of the particle-size distribution curve are assumed known and fixed. These assumptions greatly simplify the analysis to only seven variables.

The three-dimensional space presented for the data

synthesis has dimensions of length, velocity, and time. Each data point tabulated has been normalized to the 10°C model using a ratio of experimental conditions to those of 10° C water. For instance,

$$D^* = \frac{\left(\frac{\rho_M \gamma_M'}{\mu_M^2}\right)^{\frac{1}{3}}}{\left(\frac{\rho_L \gamma_L'}{\mu_L^2}\right)^{\frac{1}{3}}} D_M \qquad (10)$$

where the the subscript $_M$ represents the laboratory and the subscript $_L$ the 10° C water. The dimensional variables plotted are those values that would be seen in 10° C water. Thus the dimensions allow the reader to grasp the relative size of bed forms and conditions of experimental runs, while still allowing normalization of parameters. Yalin and Russell (1965) explicitly state ρ = constant and μ = constant for water experiments on oscillatory-flow regimes. Unfortunately this is reasonable only for ρ. The variablity of μ for water is too large to ignore over the temperature range of experimentation. The value of μ at 10°C is 1.3077 cp and μ at 60°C is 0.4688 cp(CRC Handbook of Chemistry and Physics, 59 ed.,1979.).

The difference in the exponent of μ in the three parameters is important to note since it results in a non-uniform scaling of the three variables of interest. Length variables (D, 2a, etc.) scale as the 2/3 power of the viscosity while T and U_m scale as the 1/3 power of the viscosity. For a 60°C experiment this yields a scaling

ratio of approximately 2:1 for length scales (see Southard, Boguchwal, and Romea, 1980). Of course all other variables scale accordingly at the same time. This procedure reduces scatter in the data but more importantly provides an accurate view of the stability regions of sediment bed phases.

The technique applied in the analysis is both appropriate and useful to the study of sediment bed configurations. By scaling all the forces, dimensions, velocities, etc. and equating them using these dimensionless relationships one obtains a scale model of an oceanic or lacustrine environment. This enables the production of bed forms much larger than would otherwise be possible without building an unrealistically large apparatus. As a result a large range of flow conditions are reproducible by changing the viscosity of the fluid or any other easily changed variable in the dimensionless parameters. In any sedimentological analysis the observed variables must have a simple relationship to a natural flow regime.

The application of this dimensional analysis to the work of other investigators is possible only with those that record temperature. Temperature data from the work of Kennedy and Falcon (1965), Carstens et al. (1969), Mogridge and Kamphuis (1972), and Lofquist (1978) were either recorded in the published work or obtained by the writer. The application of the data synthesis brings a change in the relative position of data points for Carstens et al. (1969)

and Mogridge and Kamphuis (1972) in which temperature was varied from one experimental run to another. For the other two investigations it serves only to scale up the results uniformly, but it is relevant when compiling a complete list of data sets. Tables 5 through 8 in the appendix show only the dimensionless parameters for each run; raw data are not included.

Equation of Motion

For this study it is assumed that the temporal velocity pattern is sinusoidal. Mogridge and Kamphuis (1972) note that oscillatory flow is rarely sinusoidal due to mass transport. The mass transport distance ξ, the net distance moved by the fluid outside the boundary layer, is a nonlinear unpredictable term in the equation of fluid motion. Its relative effect on fluid motion is small. Mogridge and Kamphuis (1972) define an effective orbital length A as

$$A = 2a + |\xi| \tag{11}$$

A is then used in dimensionless parameters to characterize the flow. For the sake of simplicity A, as defined by Mogridge and Kamphuis, is assumed to be equal to the observed excursion of a fluid particle. The effect on U_m is negligible.

The other important factor on the shape of the temporal velocity profile is the time-varying flow resistance. Within the boundary layer the flow is affected nonlinearly by τ_m, since τ_m grows approximately as the square of U_m in the range of flow encoutered in this study. The anticipated velocity pattern is one with lower acceleration and deceleration on either side of the velocity maximum. Attempts in the experimental program to measure the temporal velocity pattern failed. Thus in the following analysis it has been assumed to be sinusoidal and similar to that produced under free-surface gravity waves.

The equation of motion for the fluid can be written

$$\frac{\partial U}{\partial t} = \frac{\partial U_1}{\partial t} + \nu\frac{\partial^2 U}{\partial z^2} - \frac{\partial \overline{uw}}{\partial z} + U\frac{\partial U}{\partial x} \qquad (12)$$

where u and w are velocity fluctuations in the x and z directions, respectively. For laminar flow the velocity-fluctuation terms go to zero and a solution can be obtained. No solution has been found yet in the case of turbulent flow (Jonsson, 1966). For oscillatory flow the acceleration terms in the x-direction dominate the equation of motion. The equation of motion is affected by the presence of bed forms in that the term for $U(\partial U/\partial x)$ becomes significant. With a plane bed $U(\partial U/\partial x)$ can be ignored, but for a wavy surface, the equation of motion becomes difficult to solve because of this nonlinear term.

In oscillatory flows due to waves the bottom boundary experiences a flow effect known as streaming. Streaming is a circulation pattern in the flow that results from mass and momentum conservation in a spatially and temporally varying velocity field. As a free-surface gravity wave passes over the bottom at some point X_1, a point in front of X_2 experiences a different velocity field than X_1 at the same instant. Two such points spaced sufficiently far apart, $|X_2-X_1| > 2a$, will at different times have convergent and divergent velocity vectors (Figure 2). This fact is responsible for wave-induced streaming over a sediment bed.

Streaming in the flow can also occur in response to the local bed configuration. If surface elements on the bed are sufficiently tall, flow separation around them produces the

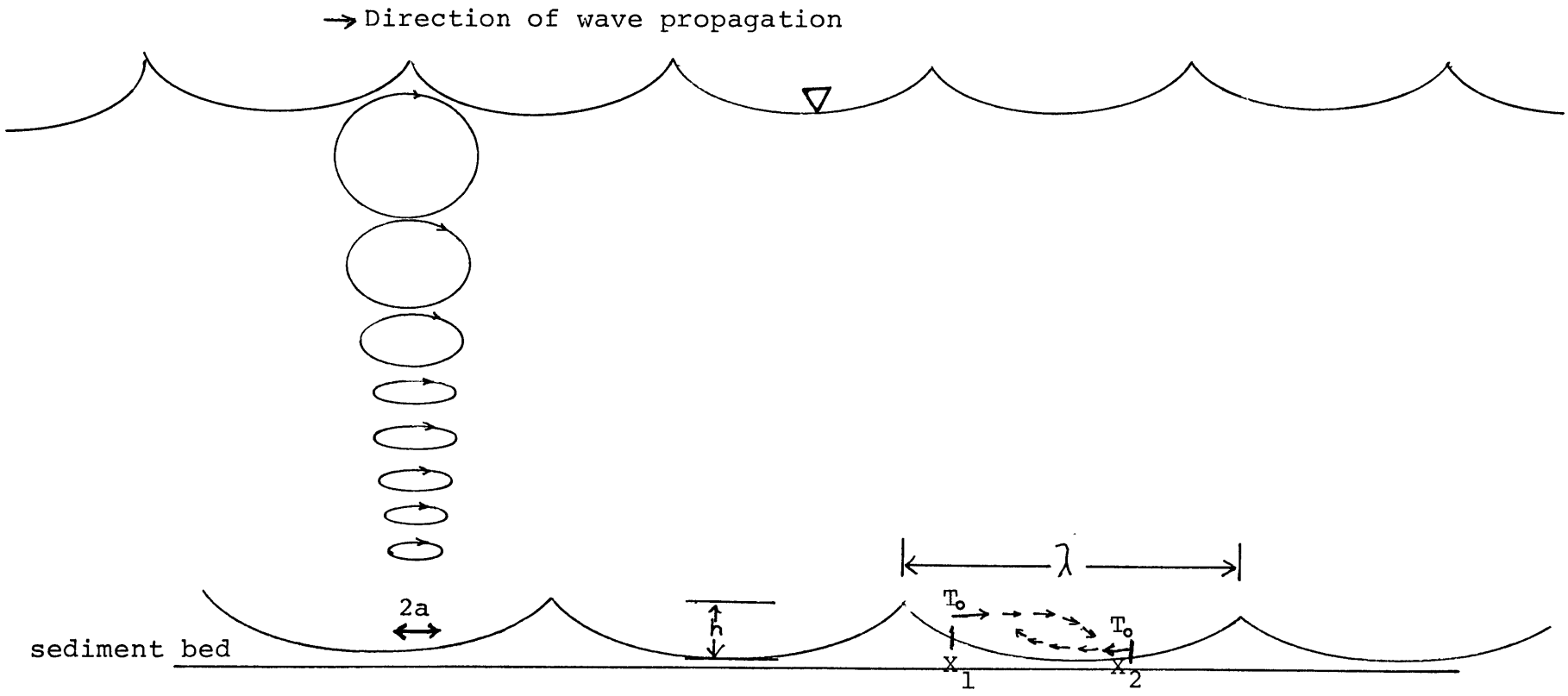

Figure 2: Oscillatory flow over a sediment bed.
(Note: Ripples drawn out of scale to demonstrate wave induced streaming; 2a is greater than λ.)

same sort of convergent and divergent velocity field as that of a free-surface gravity wave. In two important papers on theoretical flow-recirculation patterns over a wavy surface, Lyne (1971) and Sleath (1975) consider different flow conditions and bed configurations and their resultant flow fields. Lyne (1971) considers a flow parameter kR which represents the ratio of 2a and λ. The streaming term in the flow, denoted $F_1^{(s)}$, is

$$F_1^{(s)}(\eta) = f_1^{(s)}(\eta) + f_1^{(s)}(\eta) \qquad (13)$$

where $\eta = \Phi(\omega/2\nu)^{1/2}$ (i.e. the velocity potential divided by the boundary-layer thickness). Three possible cases for the flow are then mathematically solved using conformal mapping. The first is for $kR<<1$ but $k>>1$. Steady streaming is confined to the boundary layer, whose thickness is of the order of a wavelength (Lyne, 1971). For the next case Lyne takes $kR<<1$ but now $k<<1$ (i.e., wavelength of the wall is much smaller than the thickness of the boundary layer). The streaming term then contains two terms: one that decays to zero over the length scale of the boundary layer and one that decays over a much larger length scale, of the order of a wavelength. Two recirculation cells form which match across $\eta=1$ (Figure 3b). The final case considered is for $kR>>1$ (i.e. $2a>\lambda$) while the viscous-sublayer thickness is of the order of $1/(kR)\ \delta$. The steady streaming associated with this flow consists of multiple recirculation cells all of equal thickness and confined to the boundary layer. The relative magnitude of

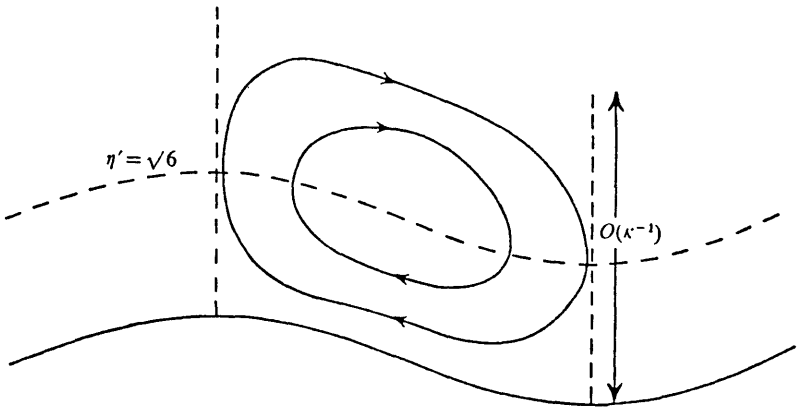

Figure 3a: Sketch of steady streaming when $kR \gg 1$ and $k \gg 1$.

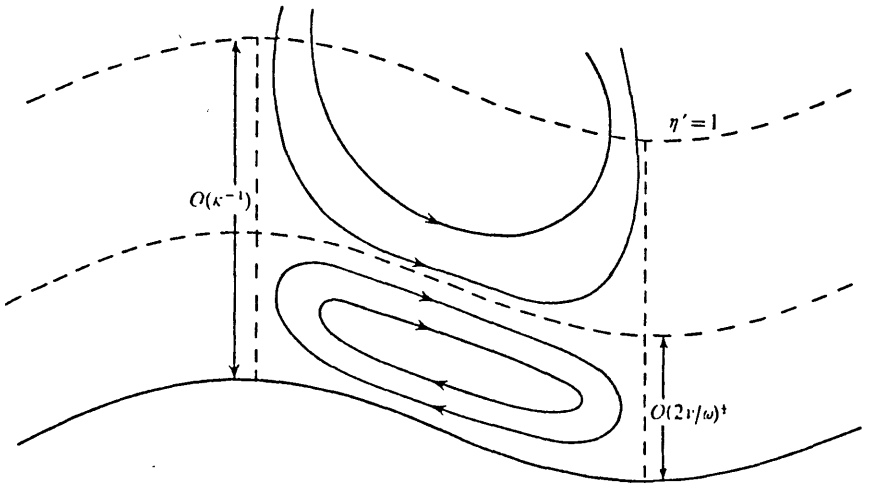

Figure 3b: Sketch of steady streaming when $kR \gg 1$ and $k \ll 1$

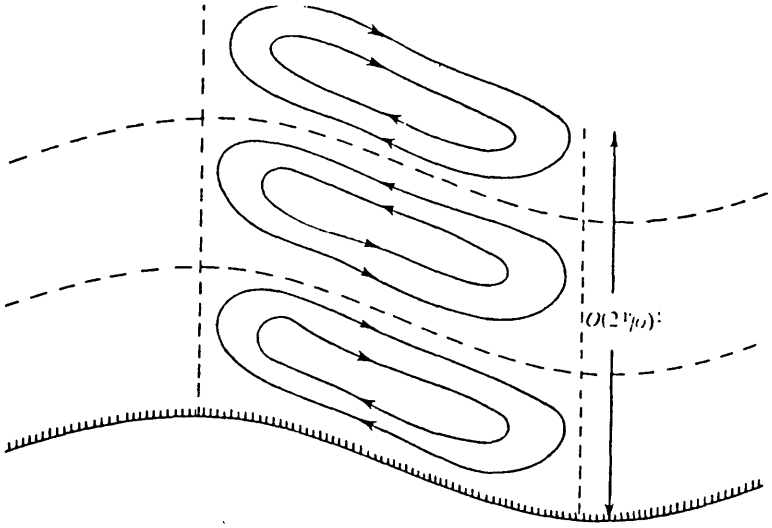

Figure 3c: Sketch of steady streaming when $kR \ll 1$ and $k(kR) \sim O(1)$ after Lyne (1971)

recirculation decreases exponentially away from the wall (Figure 3c). All three cases produce recirculation cells that transport material or impinge on the bed with velocity vectors directed toward ripple crests.

Sleath (1975) made a similar study of the velocity field under oscillatory flow. Like Lyne he solved for laminar flow, in which fluid movement is mathematically predictable. The result of the study is a mathematical prediction of the velocity at a point on the bed. The velocity vector is always toward ripple crests and is independent of time.

The apparatus used in the present study did not produce the streaming induced by free-surface gravity waves. The second type of streaming, that produced by ripples on the sediment surface, was present in the laboratory experiments of this study. The limit of such streaming was the top surface of the duct. If bed-form height was sufficient the flow felt the top of the duct and was squeezed over the ripple crests. This enhanced recirculation and led to unrealistic bed forms. The rule of thumb employed was a height clearance over the ripple forms of $1/2\ \lambda$. Below this the recirculation cells were spatially restricted and the $U(\partial U/\partial x)$ term was too large for accurate reproduction of the flow environment.

Boundary Layer Theory

The boundary layer in an oscillatory flow is limited in thickness because of the short time in which it grows and

decays. Conversely, in unidirectional flow the boundary layer grows until it reaches a free surface. It has long been assumed that unidirectional-flow boundary layers have a logarithmic velocity profile that is steep near the boundary and nearly constant up in the flow. However, an oscillatory boundary layer develops and decays within a half-period of oscillation, making its velocity structure irregular. Yet, it is clearly a function of frequency. The boundary-layer thickness δ for laminar oscillatory flows is

$$\delta=\left(\frac{\pi}{4}\right)^{\frac{1}{2}}\ (\nu T)^{\frac{1}{2}} \tag{14}$$

Sleath (1974) uses the roughly equivalent expression

$$\delta=\left(\frac{\omega}{2\nu}\right)^{\frac{1}{2}} \tag{15}$$

and suggests that flow may remain laminar under conditions of practical importance. The flow may in fact be turbulent but the mean-velocity distribution may still be represented by solutions for the laminar case.

Two important length scales exist for oscillatory-flow boundary layers: the boundary-layer thickness δ and the orbital diameter 2a. Two unique Reynolds numbers can be constructed using these variables:

$$\mathrm{Re}=\frac{U_m\delta}{\nu} \tag{16}$$

$$\mathrm{RE}=\frac{U_m a}{\nu} \tag{17}$$

The use of a boundary-roughness Reynolds number (Re) should be restricted to analysis of the flow in the boundary layer.

However, the mean-flow Reynolds number (RE) is useful both inside and outside the boundary layer; the mean flow controls the boundary shear stress because of velocity matching across the transition.

Transfer of momentum between fluid layers is governed by viscous effects such as vortex formation and decay. The boundary shear stress, which controls sediment movement, is governed by the thickness of the boundary layer. Jonsson (1966) discussing the case of rough turbulent flow, derives an expression for δ using the early work of Nikuradse on bed roughness k_s. The expression relates the boundary-layer thickness to the bed roughness and the orbital radius, a. Jonsson uses a value of k_s equal to 3 or 4 times the bed-form height h, but this value is arbitrarily determined from experimental work. Madsen and Grant (1982) review the literature and cite a range of values from h to 4.7 h. The best value for this coefficient is taken to be 2.5 for the calculation of boundary-layer Reynolds numbers.

Jonsson (1966) defines the boundary-shear stress τ_m as a function of a friction factor f_w:

$$\tau_m = f_w(1/2)\rho U_m^2 \tag{18}$$

The boundary-layer thickness can then be found from the equations

$$U^* = \left(\frac{\tau_m}{\rho}\right)^{\frac{1}{2}} \tag{19}$$

$$\delta = \frac{\kappa U^*}{\omega} \tag{20}$$

For laminar flow the gradient of the boundary shear stress is

$$\left.\frac{\partial \tau}{\partial z}\right|_{z=0} = -\rho\frac{\partial U}{\partial t} \qquad (21)$$

where $U = U_m \sin\omega t$ (Jonsson, 1966). Because of the relative thinness of the oscillatory-flow boundary layer, the gradient becomes very large over the length scale δ. Therefore the velocities required to move sediment under an oscillatory flow may be as much as an order of magnitude lower than for unidirectional flow.

Unfortunately, an exact solution to the equation of motion has not been obtained for turbulent oscillatory flow because it involves a nonlinear differential equation. Jonsson obtained solutions of the boundary shear stress for turbulent flow after assuming a logarithmic velocity profile across the boundary layer (a reasonable assumption based on his own experimental measurements of the velocity profile).

Threshold of Sediment Motion

In a few runs there was no movement on the sediment bed. Several investigators have made theoretical predictions of the threshold of sediment motion in oscillatory flows. The most recent and mathematically rigorous equation comes from Komar and Miller (1974). They find that for $D < 0.05$ cm

$$\frac{\rho U_m^2}{(\rho_s - \rho)gD} = 0.21 \left(\frac{2a}{D}\right)^{\frac{1}{2}} \qquad (22)$$

at conditions of incipient sediment motion. Applying this equation to the two sands used in this study generates a curve that passes above the first grain movement seen (see Figures 4 and 5).

Komar and Miller's curve is an empirical one with a theoretical basis. Unfortunately the fitting was done to Bagnold's (1946) data set. Bagnold (1946) used an oscillating sediment tray, which as noted earlier produces a very different flow profile above the bed from that of a moving-fluid system. The no-movement points produced using the coarser sand indicate a positive slope for the no-movement boundary.

The problem in the fit of the predicted curve may result from the absence of scale modelling in analyzing Bagnold's data. The slightest change in the empirical coefficient (0.21) moves the boundary a great deal. The remainder of equation (22) is based on the forces acting upon a grain under an oscillatory flow. The fit of the slope with the data obtained (Figure 4) is a good indicator that the fundamental factors involved in moving sediment have been included. The use of water at a temperature above the 10° C normalization used here would alter the fitting parameter and account for the discrepancy in observed first motion. The effect of scaling Bagnold's data would be to increase the velocity and period slightly (assuming he did his work with room temperature water).

Another possible factor in the discrepancy between the

writer's data, and the curve shown by Komar and Miller is the streaming phenomena previously described. The lack of streaming forces from free-surface gravity waves reduces the recirculation patterns outside the boundary layer and thus increases the relative velocity at the bed. This results in a higher boundary shear stress. The end effect is that sediment may move in an oscillatory-flow duct at lower velocities than under free-surface gravity waves.

The data from this and other studies suggest that the no-movement curve has a positive slope. At larger periods greater velocities are needed to initiate sediment movement. This is predictable from the boundary-layer thickness δ. The variable δ has a direct relation to T. Thus for two runs with the same U_m, a higher value of T lowers the bed shear stress τ_m because of the increase in δ.

The initiation of grain motion is most dependent on bed shear stress in oscillatory flow. The curve of incipient motion in oscillatory flow relates the friction forces on the sediment grains to the particle weight of the sediment based upon grain diameter. The two components of bed force, skin friction and form drag, are of different orders of magnitude in oscillatory flows capable of moving sediment. Form drag predominates for bed forms. For sediment grains, form drag may or may not predominate over the skin friction depending on the flow structure around the grains on the sediment bed. The grain friction on the flow is important to the bed shear stress at least locally; therefore a

variable like Nikuradse's k_s is appropriate for determining flow resistance due to sediment grains.

Komar and Miller (1973) have related bed shear stress to the grain roughness. In so doing they have applied the same line of thinking that produced the Shields' curve of unidirectional incipient motion. The appropriateness of the variables is hardly arguable in light of the wealth of data that support the calculated transition. τ_m is a fairly uniform and continuous function of T and U_m over a large range of the variables. The discontinuous changes in τ_m that occur when flow conditions change from smooth turbulent to rough turbulent are not seen on the boundary between movement and no movement of grains at natural or realistic values of T. The most important forces acting upon the grains and on the fluid are summed up in Komar and Miller's curve, which predicts a coincident increase in U_m and T and U_m and D.

Discussion of Bed Forms

The lack of vortex cells in the flow is perhaps the chief characteristic of rolling-grain ripples. Development of rolling-grain ripples through preferential erosion of the sediment surface does not produce vortex action in the fluid. The continued movement of grains on the sediment surface after the ripples form and equilibrate with the flow demonstrates spatially uniform grain movement. Therefore the sediment moves but the rolling-grain ripples do not.

During development the ripples may progress along the bed or change spacing, but their form remains the same. The sediment interchange between adjacent rolling-grain ripples reaches a steady-state equilibrium. When the ripples were seen as only a brief transitory bed configuration in an experiment the presence of vortices dictated a change to some other bed configuration.

2D vortex ripples form in flows with horizontal-rotational vortices under a variety of conditions. They are relatively long-crested. The high level of nonuniform erosion and deposition results in a characteristic spacing-to-height ratio for 2D vortes ripples. The straight crests of the 2D vortex ripples were seen in other studies to produce long regular vortex cells with a passing wave surge. The scour of these vortex cells on the troughs often results in irregular ripple-shoulder profiles. The velocity shielding by ripple crests imparts a stop-start current to the sediment bed with net flow toward the ripple crests. The flow reattaches on the flank of the next ripple downstream. The recirculation of water toward the upstream ripple crest combined with the subsequent reversal in velocity surge results in irregular ripple shoulders. Depending on the flow recirculation, the irregularities were either scour pockets or small trough ripples. This phenomenon is noteworthy but was not studied in detail.

The stratification and texture produced by 2D vortex

ripples should be easily recognized in the field. The field study by Inman (1957) reported the same type of grain-size sorting observed in 2D vortex ripples in this study. The presence of coarser sand near the ripple crest agrees with the intuitive idea of a higher transport velocity for larger grains. The velocity minimum in the trough gives the greatest chance of fine-sediment accumulation. Also the interfingering laminae of stationary vortex ripples is distinctive. However, migrating 2D vortex ripples would be difficult to distinguish from unidirectional-flow ripples since they both leave foreset laminae.

The stability field for 2D vortex ripples in the parametric space used here lies above that for 3D vortex ripples with respect to T and below it with respect to U_m. The boundary between the two is reasonably well defined by the data from this study. The runs in which both ripple types appear plot in a narrow region with a positive slope (Figures 4 and 5). This interpretation of the data is subjective but is reinforced by observation of the flow at lower T and constant U_m and higher U_m and constant T. The pattern of vortex action changed across a boundary with a positive slope in U_m and T space.

The grain size appears to have an important effect on development of 2D vortex ripples. The stability region for 2D vortex ripples relative to 3D vortex ripples lies in the direction of larger D and smaller U_m (Figures 8, 9, 10, 11). The stability field for 2D vortex ripples was much

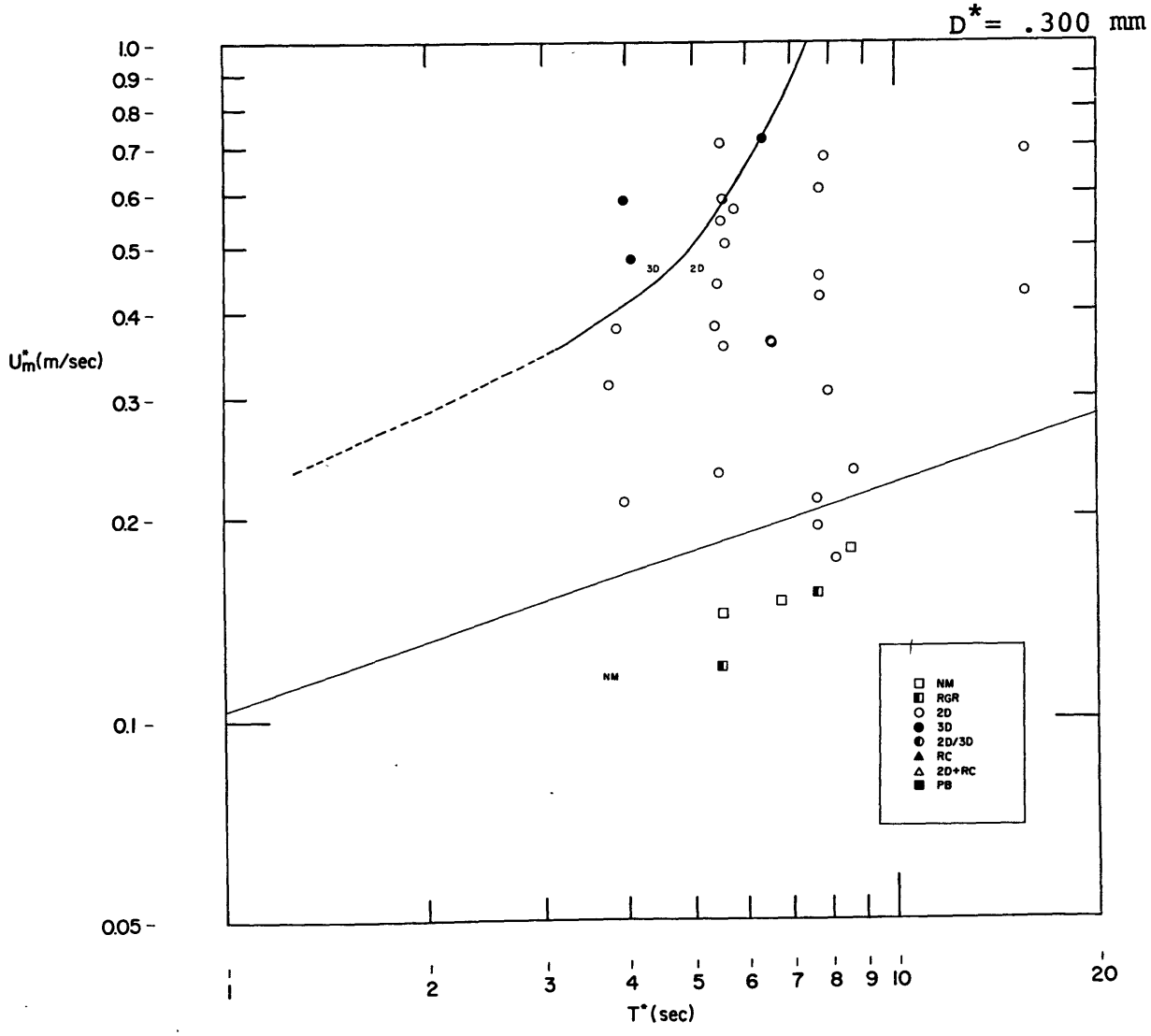

Figure 4: U_m vs. T in coarser sand.(Table 3)

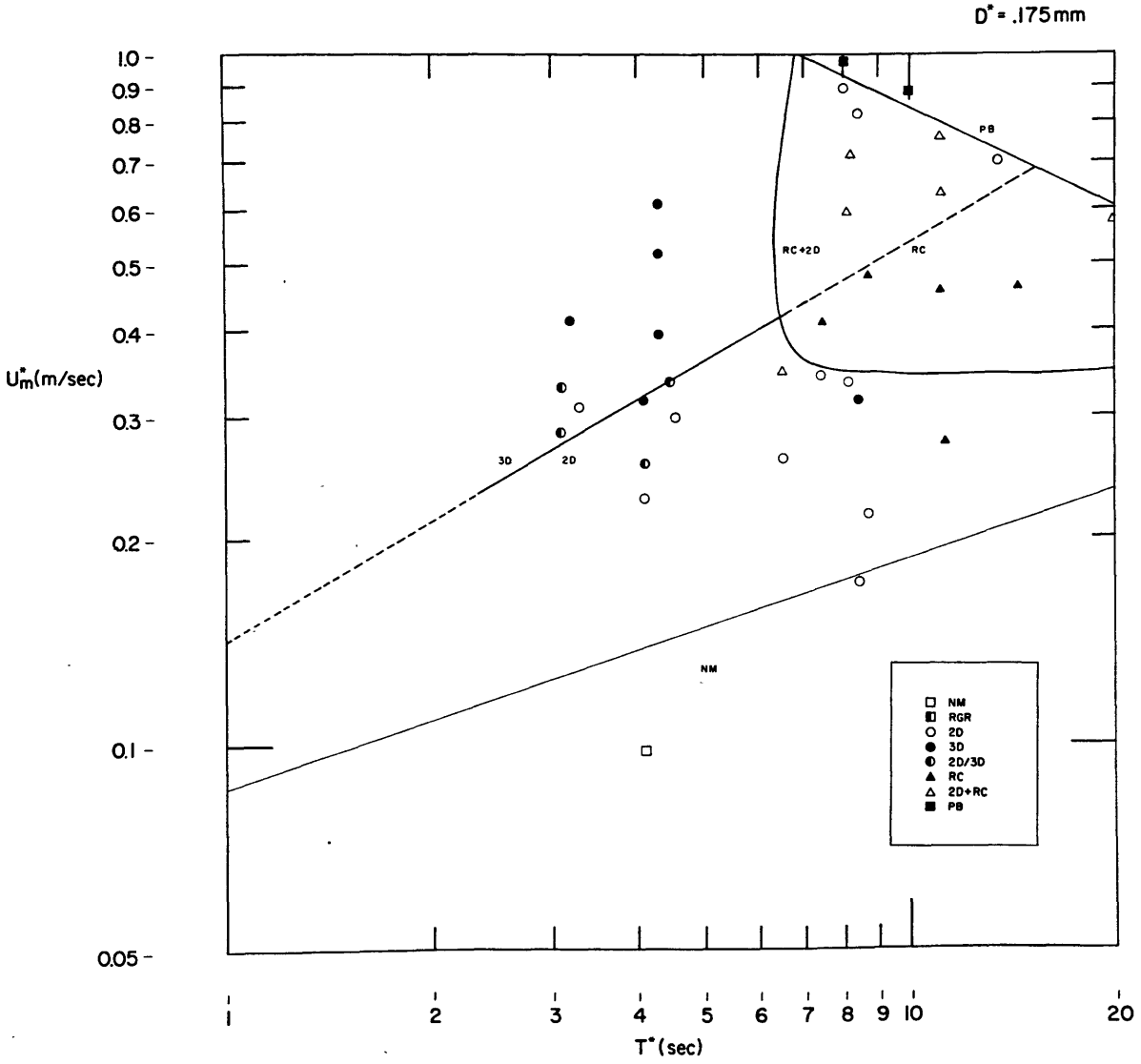

Figure 5: U_m vs. T in finer sand.(Table 4)

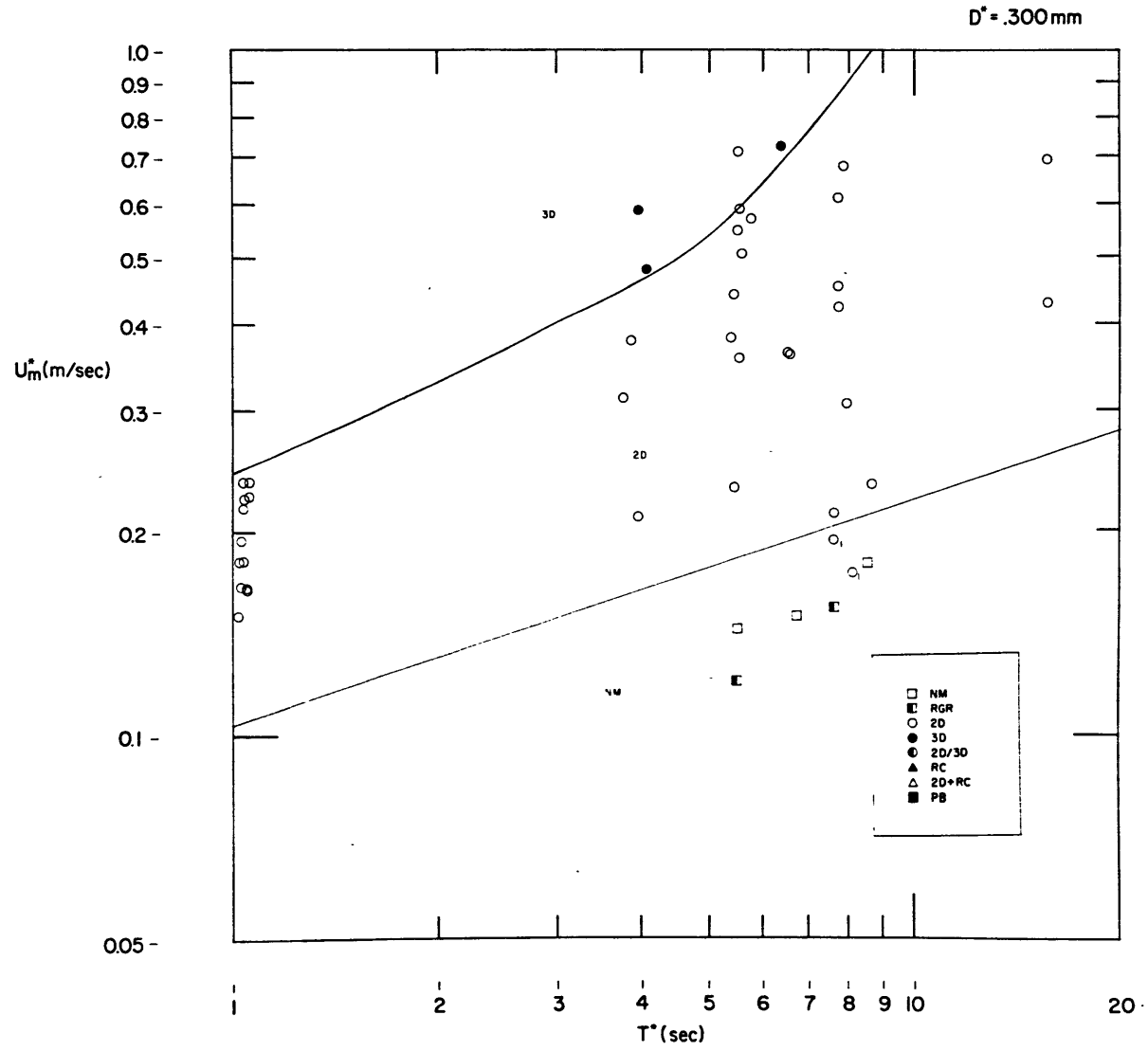

Figure 6: U_m vs. T for D= 0.300 mm.

denotes metastable 2D vortex ripples.

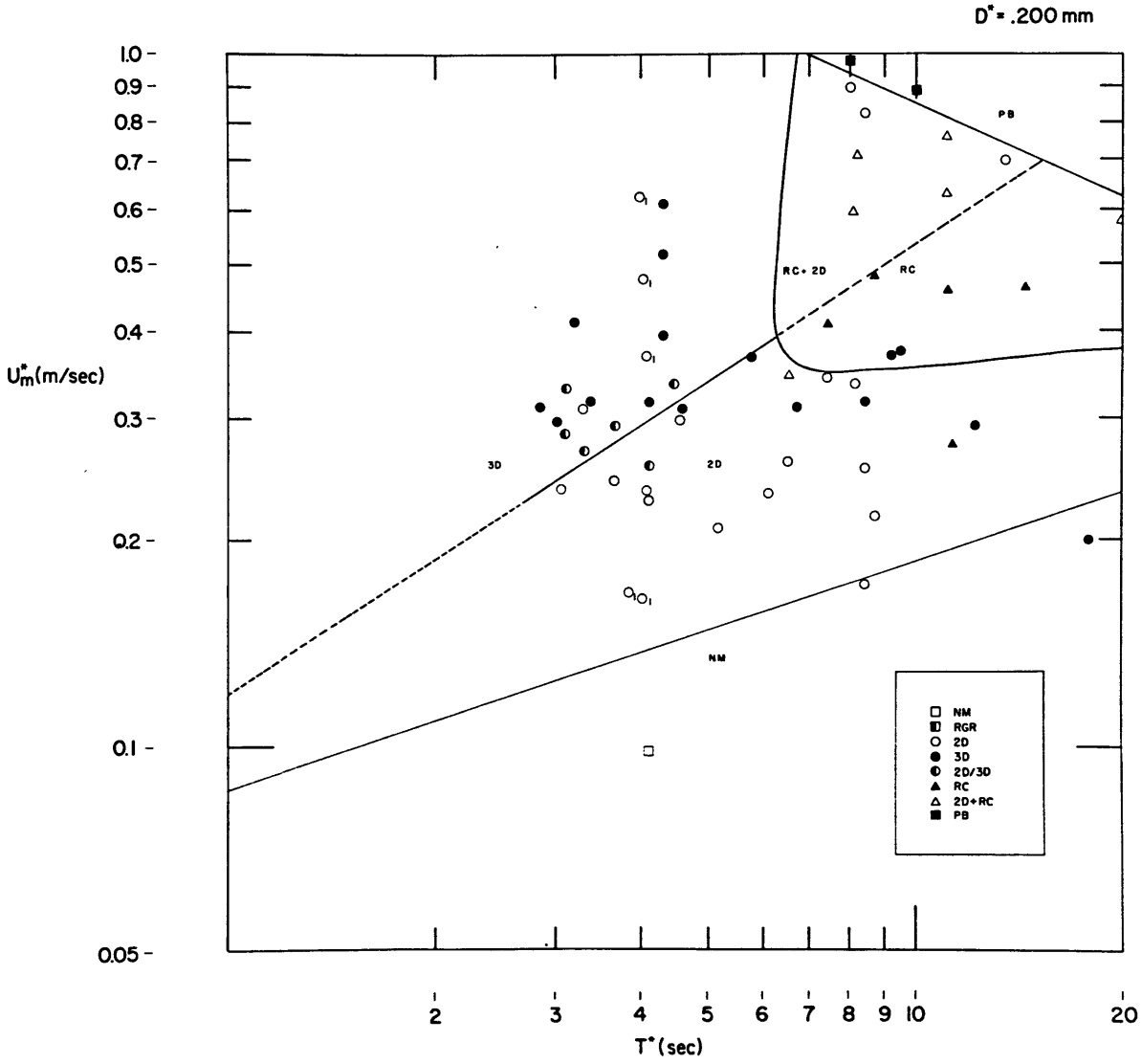

Figure 7: U_m vs. T for D= 0.200 mm.

denotes Carstens et al. experimental data.

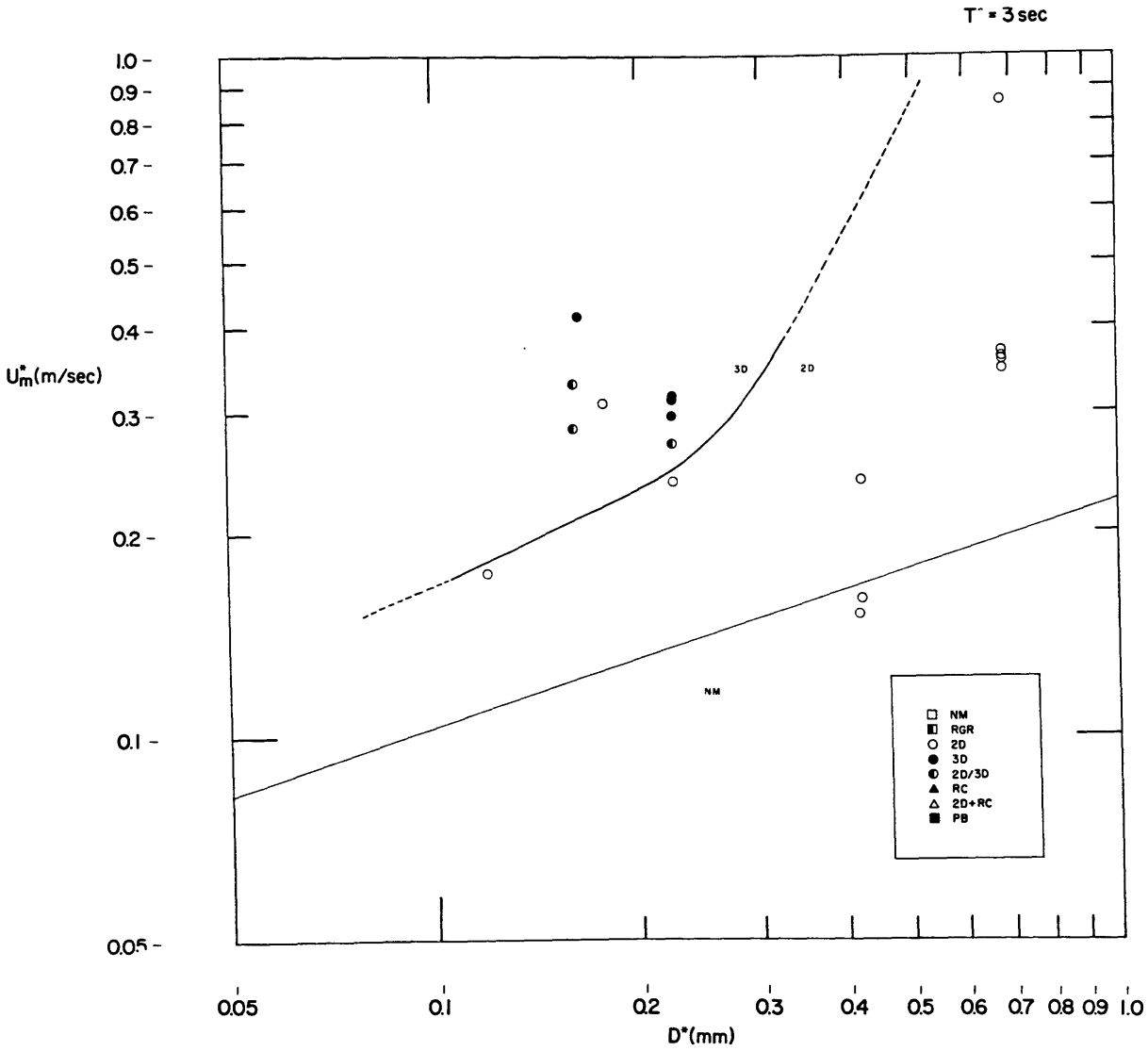

Figure 8: U_m vs. D for T= 3 s.

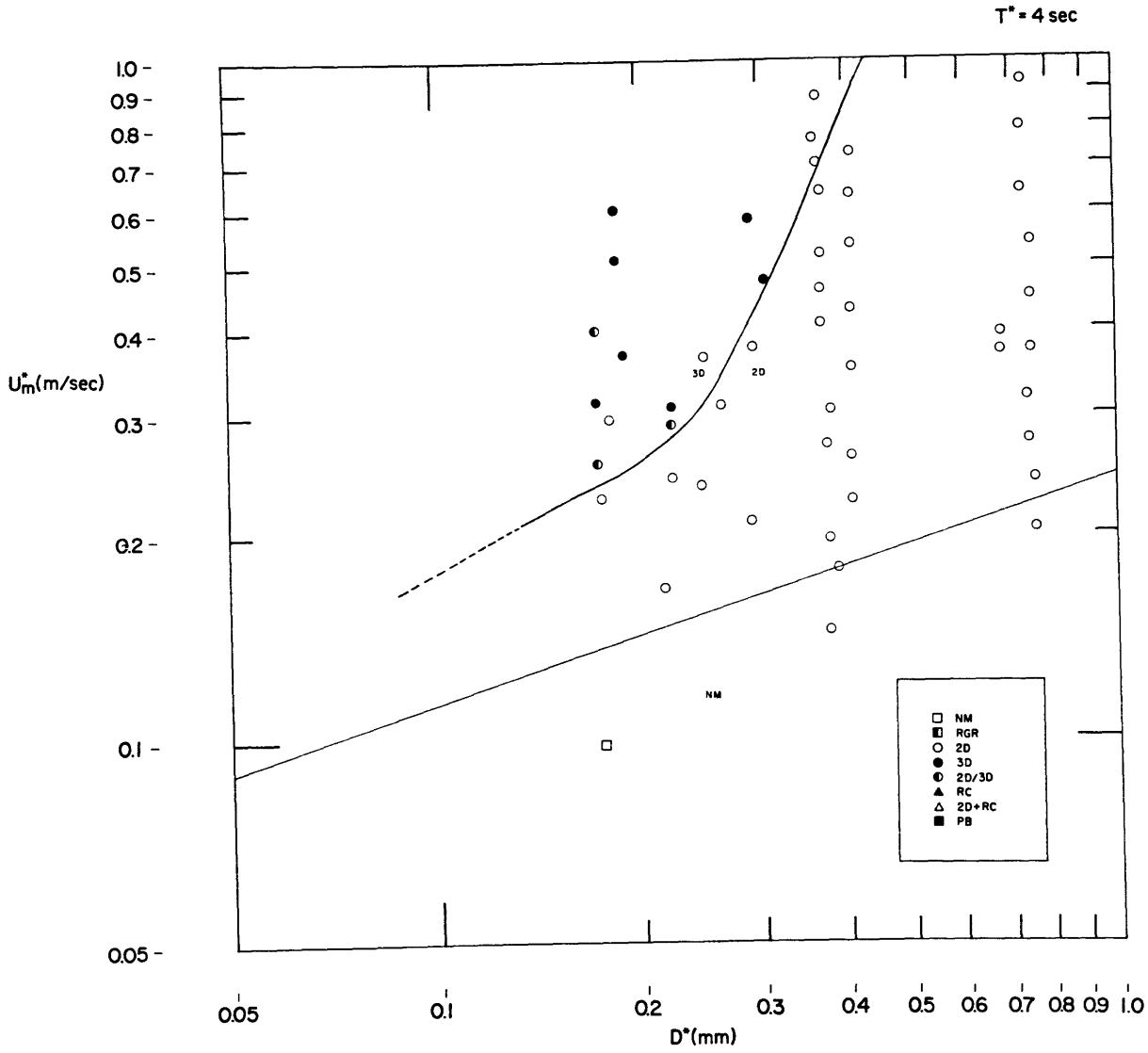

Figure 9: U_m vs. D for T= 4 s.

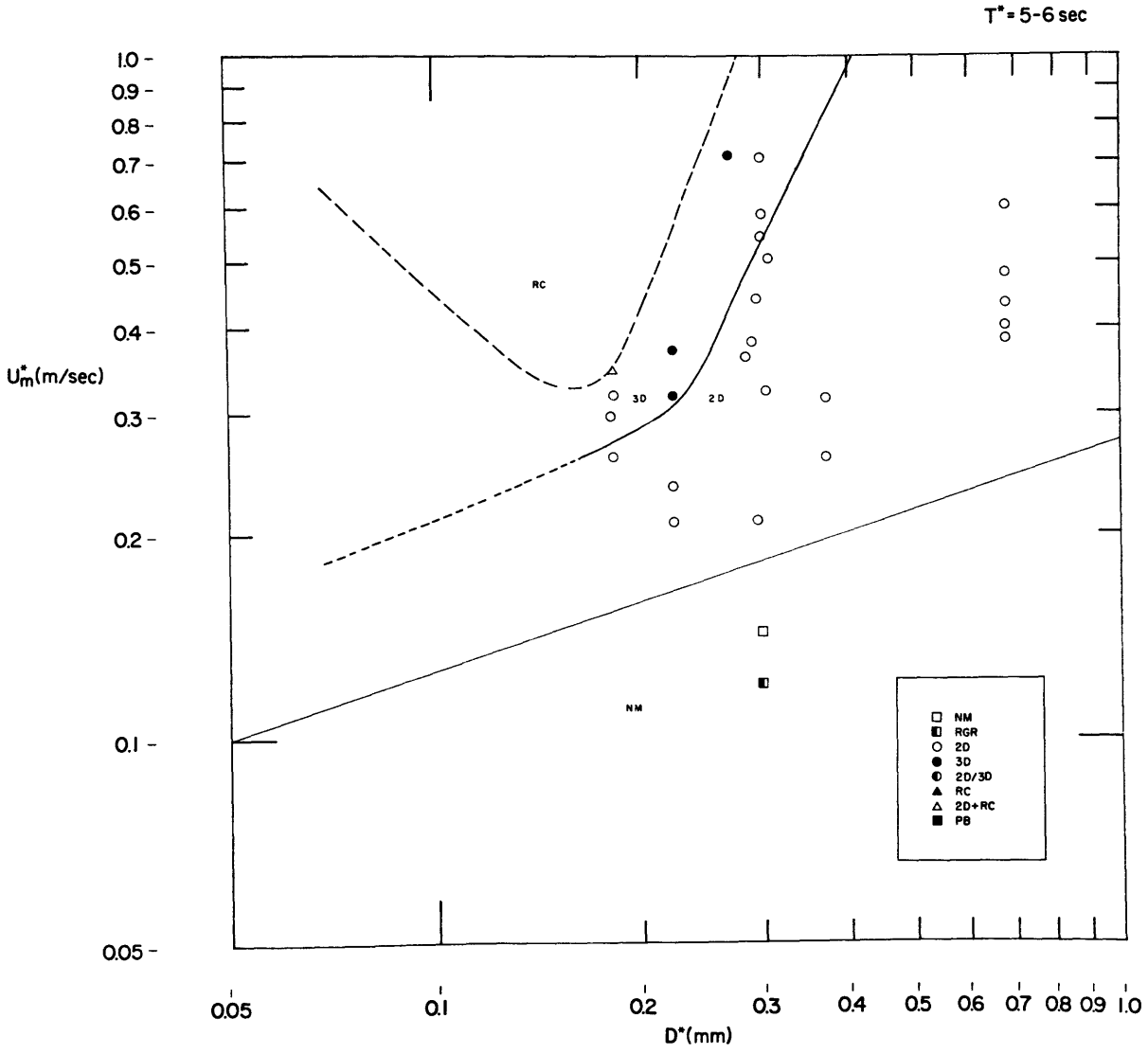

Figure 10: U_m vs. D for T= 5-6 s.

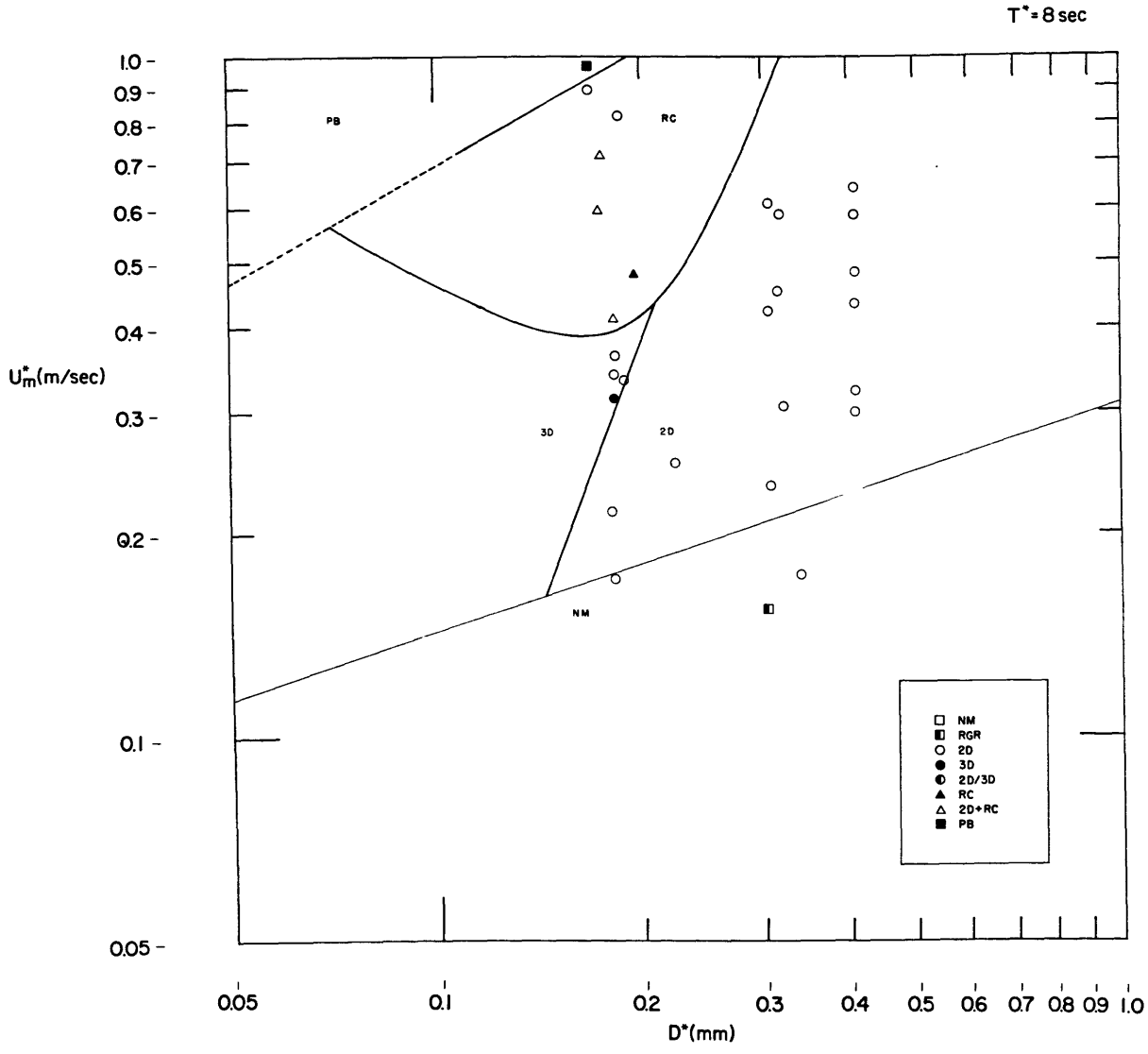

Figure 11: U_m vs. D for T= 8 s.

larger for the coarser sand. The lower boundary for development of 3D vortex ripples in coarser sands is shifted up and to the left with respect to U_m and T. This dependence on grain size may be a direct reflection of the friction felt by the flow. With a greater bed friction on the flow, less energy is dissipated in the fluid and more at the fluid-solid interface. The greater velocities required to transport coarser sands may enable the bed to stabilize with a regular geometry. Less sediment transport takes place near the zero point in the temporal velocity profile and thereby more regular sediment transport results.

3D vortex ripples have a direct relation to 2D vortex ripples: they occur at larger Um and smaller T and have an expanded stability field with smaller D. The interdependence between bed geometry and flow makes questionable any interpretation of the vortex patterns in the flow. The three-dimensionality of the vortex cells may result from irregular sediment transport across the flow direction or vice versa. The visibly stronger sediment transport per cycle over 3D vortex ripples than over 2D vortex ripples is a function of the higher energy of the flow. Perhaps at some critical level of flow conditions the fluid no longer completely specifies the spatial distribution of sediment deposition. A flow unable to reach a dynamic equilibrium with the local topography would then be subject to changes induced by the bed profile. The movement of sediment through the flow

acceleration-deceleration cycle warrants further investigation to determine the mechanism important in development of 3D vortex ripples.

Reversing-crest ripples form in an environment mechanically different from that of vortex ripples. Their resemblance in vertical profile to that of unidirectional ripples signifies the linear nature of the flow that produces them. They form at long periods ($T > 6$ s) and large U_m. This places them in the upper right-hand corner of Figure 5. The stability field for reversing-crest ripples is larger for smaller values of D. The lack of coarser-sand runs with only reversing-crest ripples is one indication of this dependence upon D.

The overlap region between vortex and nonvortex behavior is large. The supression of bed-form growth attributed to reversing-crest ripples seems to taper off with decreasing U_m. Reversing-crest ripples are stable over a relatively large overlap region. Yet it is entirely possible that long-term vortex growth would preclude reversing-crest ripples forming in the overlap region. Such a possibilty was not verifiable in this investigation. The overlap region of vortex and reversing-crest ripple growth lies in a band with a positive slope in U_m and T (Figures 5 and 7). The coupling of the mechanics of formation for the two ripple types produces a distinctive bed profile. When both bed forms are present vortex growth is limited and the eventual bed configuration is not a simple superposition of

the two ripple types but is instead a geometry concordant with both flow regimes.

Upper planar bed conditions are at high U_m and T. The orientation of the boundary between rippled beds and planar beds has a negative slope in U_m and T (Figures 5 and 7). Thus for a given U_m ripples disappear with increasing T. The strong sediment movement during each oscillation precludes even short-term bed-form stability.

Questions Addressed

One of the major questions to be addressed in this study was the growth of rolling-grain ripples into vortex ripples. The qualitative results presented indicate that rolling-grain ripples are stable at very specific conditions: they occur just after the threshold of sediment motion is crossed but even then are stable only at short periods of oscillation. The interpretation is that they are unstable for conditions in which their presence on the bed produces flow separation. The flow separates if U_m is large enough, so 2D vortex ripples will develop from rolling-grain ripples. At small enough U_m and T the flow is strong enough to move sediment grains on the surface but vortices do not develop behind the rolling-grain ripples formed.

Vortex ripples are stable below the threshold for no-movement on a planar bed. The series of runs made with the coarser sand in which U_m was systematically decreased

confirmed the stability of 2D vortex ripples at low U_m. Runs 20-25 (Tables 1 and 3) represent this sequence. As sediment transport diminished, vortex ripples were maintained while their spacing and height decreased. The seemingly anomalous data points of Graph 1 do not affect the interpretation of the threshold of sediment motion; the final bed form for each run appears in the table of values, and these stable 2D vortex ripples were a result of earlier runs. Run 26 was started with a plane bed and represents the bed configuration produced from such conditions. 2D vortex-ripple stability below the threshold of sediment movement is perhaps a result of the flow disturbance produced by their presence on the sediment bed. Clearly the capability of the flow to transform the bed configuration diminishes at lower energy conditions; this is probably the most significant factor in this phenomenon of metastable 2D vortex ripples.

The implication of this simple result to ancient sedimentary strata is important. Vortex ripples produced during episodic events out on the continental shelf, or some other deep-water environment in which the typical free-surface gravity wave does not move sediment on the bottom, might remain in the sedimentary record. One would expect to see vortex-ripple laminae covered by low-energy deposits. Rolling-grain ripples would be seen only if flow conditions came up from no-movement to rolling-grain ripple stability. Descending in U_m and T would produce 2D vortex

ripples that dominate down to the no-movement threshold. Of course higher-energy bed forms could be produced during such an event, but in the end flow conditions would pass through the 2D vortex-ripple stability field. In some cases 2D vortex ripples take only 2-4 hours to develop completely. Thus unless there is rapid aggradation the record of high-energy environments is erased by the development of lower-energy 2D vortex ripples.

The transition from vortex ripples to nonvortex, reversing-crest ripples happens at high values of T. The formation of reversing-crest ripples seems to involve no flow streaming. The stability of vortices breaks down at the transition from vortex ripples to nonvortex ripples. Flow velocities for nonvortex ripples are high, but they produce nonvortex ripples only when T is also large. This restricts the stability field for nonvortex ripples to the upper right-hand corner of Figures 4, 5, 6, and 7. The transition from the one form to the other is not abrupt; vortex and nonvortex ripples coexist over a wide range of conditions . Vortex ripples do not develop at moderate Um and high T , indicating a breakdown in vortex stability within the flow. At lower T and higher U_m, the overlap of the two styles of bed form is clear.

For flows in which both reversing-crest ripples and vortex ripples developed, the instantaneous appearance of reversing-crest ripples indicates an independence between initial bed configuration and reversing-crest ripple

development. Conversely, the relatively slow development of vortex ripples over time reflects a dependence between flow environment and bed configuration for this phenomenon. The gradual evolution of vortex ripples is a function of a feedback loop from small ripples to flow peturbation to nonuniform erosion, which produces larger ripple forms.

The end result of development of the two coexisting bed forms is a bed with low-amplitude vortex ripples and normal reversing-crest ripples. The interpretation of this is intuitive rather than theoretical. The presence of reversing-crest ripples may smooth out the streamwise variation in sediment transport and deposition, thus explaining two observed effects. Supression of the preferential erosion caused by vortex action would explain the diminished bed heights for vortex ripples in flow regimes with a combination of bed forms. The same effect would increase the time necessary for vortex-ripple formation. Increased vortex-formation times were seen in all runs with 2D vortex ripples and reversing-crest ripples present together. Equilibrium took tens of hours rather than the 4 to 6 hours for simple vortex-ripple beds.

At high-energy conditions hysteresis effects appear to be unimportant. The flows at moderate U_m and T are affected by the bed geometry, but the consistency of results would indicate that U_m and T ultimately control the bed configuration and not vice versa. Though bed configuration does affect the flow around bed forms and the transport of

sediment, it does not affect the amount of material in suspension or that transported as bed load to the same extent as U_m and T. Bed forms and flow coexist in a sympathetic relationship. Runs initiated with identical flow conditions but different bed configurations were altered to the same final bed configuration (except in the case of metastable vortex ripples).

In the case of the transition from vortex ripples to nonvortex ripples no hysteresis effect appears to control bed configuration. Beds with vortex ripples do not supress development of reversing-crest ripples. Reversing-crest ripples form as soon as T reaches a high enough value at moderate to high U_m. The bed topography has less effect on the growth of the boundary layer in long-period oscillations. Accordingly, reversing-crest ripples grew immediately whenever flow conditions were suitable for growth.

The transition zone between reversing-crest ripple stability and vortex-ripple stability reveals a synergistic relationship between the two bed forms. The presence of reversing-crest ripples inhibits the growth of vortex ripples when the two are stable together. Vortex formation depends on the combination of gross flow conditions and bed configuration, present at the time. When reversing-crest ripples cease to move, vortex cells grow rapidly and exert control over the bed geometry.

Another of the principal objectives in this

investigation was to study and characterize nonvortex ripples at large values of U_m and T. Having described the depositional pattern of reversing-crest ripples the next step is to discuss the character of the flow. Perhaps the lack of vortices in the flow is due to the uniform erosion of the sediment bed. The build-up of large ripples in the sediment surface is then supressed by the high level of sediment movement for each half-cycle. This even erosional pattern is a characteristic of the flow that can be quantified.

The relationship between 2D and 3D vortex ripples is a complicated one. 2D vortex ripples form at lower values of U_m than 3D vortex ripples at the same T. At higher values of T, 3D vortex ripples form at larger values of U_m. The transition zone between the two ripple types is an indistinct region in U_m vs. T space (at constant D). The transition zone has a positive slope and marks a change in the nature of flow above the bed. The change in ripple geometry was seen gradually in three groups of runs using the finer sand. At some point 3D vortex ripples dominate the bed configuration, but for a small region of U_m and T space the two are coexistent and local effects influence which bed form develops. Lofquist (1978) reported many runs in which sections of the bed were 2D vortex ripples and others 3D vortex ripples. This may have been a result of the experimental configuration, but the same phenomenon was seen in this study. As mentioned in the results some 3D

vortex ripples had a characteristic spacing and height. The flow above such beds contained irregular vortex cells with linear rotational axes. Strictly 3D vortex-ripple beds occurred with flows in which vortex cells had 3D rotational axes.

Given the turbulent nature of the flow for both 2D and 3D vortex ripples it is extremely difficult to predict the flow mathematically. In simply observing the growth of the two bed forms one sees that nonuniform erosion induces rolling-grain ripple development and the flow disturbance builds up the ripples on the bed. Once fully grown, 2D vortex ripples reach a stable equilibrium with the flow, and grow and move only very slowly. 3D vortex ripples on the other hand are everchanging because the feedback loop never reaches any sort of quasi-steady-state equilibrium. The difference in vortex pattern is self-determined by the energy of the flow. The short time period in which water motion stops, coupled with the flow disturbance introduced by the bed forms, causes random vortex patterns in 3D flow. The cause of 3D vortex ripples may lie in the inability of the flow to dissipate energy smoothly.

The transition from vortex ripples to plane bed is a distinct region at high U_m. The period T has some effect on the position of the boundary but, U_m seems to be the dominant flow parameter. Planar beds form from vortex ripples or from reversing-crest ripples at different values of T. The value of T marking this boundary is approximately

7 s. Below 7 s the change from vortex ripples to planar bed entailed a change from flow in which vortex cells regularly appeared, to flow in which no disturbance was seen at all, in spite of the suspended load that provided visualization. Above 7 s reversing-crest ripples become smaller near the transition to a planar bed, until at high U_m they no longer develop. Planar bed configurations contain no finite elements on the bed at any point in the oscillatory cycle. Vortex ripples could not be maintained against the uniform erosion of the sediment surface in planar-bed flows. Vortex ripples were quickly eroded away and their sediment entrained and redistributed over the whole bed in a planar layer. The high U_m and T values needed for planar bed configurations limits the availability of data points. One would anticipate planar beds at lower U_m and very high T.

Speculation

The calculation of RE near the threshold of sediment movement observed in this study is revealing. The transition from no movement to rolling-grain ripples or 2D vortex ripples occurs at values of RE near the line between laminar flow and laminar-to-smooth turbulent flow in the boundary layer (Figure 12). This zone has two physically meaningful characteristics: it exists for small values of a and k_s, and it exists only for relatively small a/k_s. The low values of a and U_m are easily understood as representing low-velocity flows, but in addition they require a third

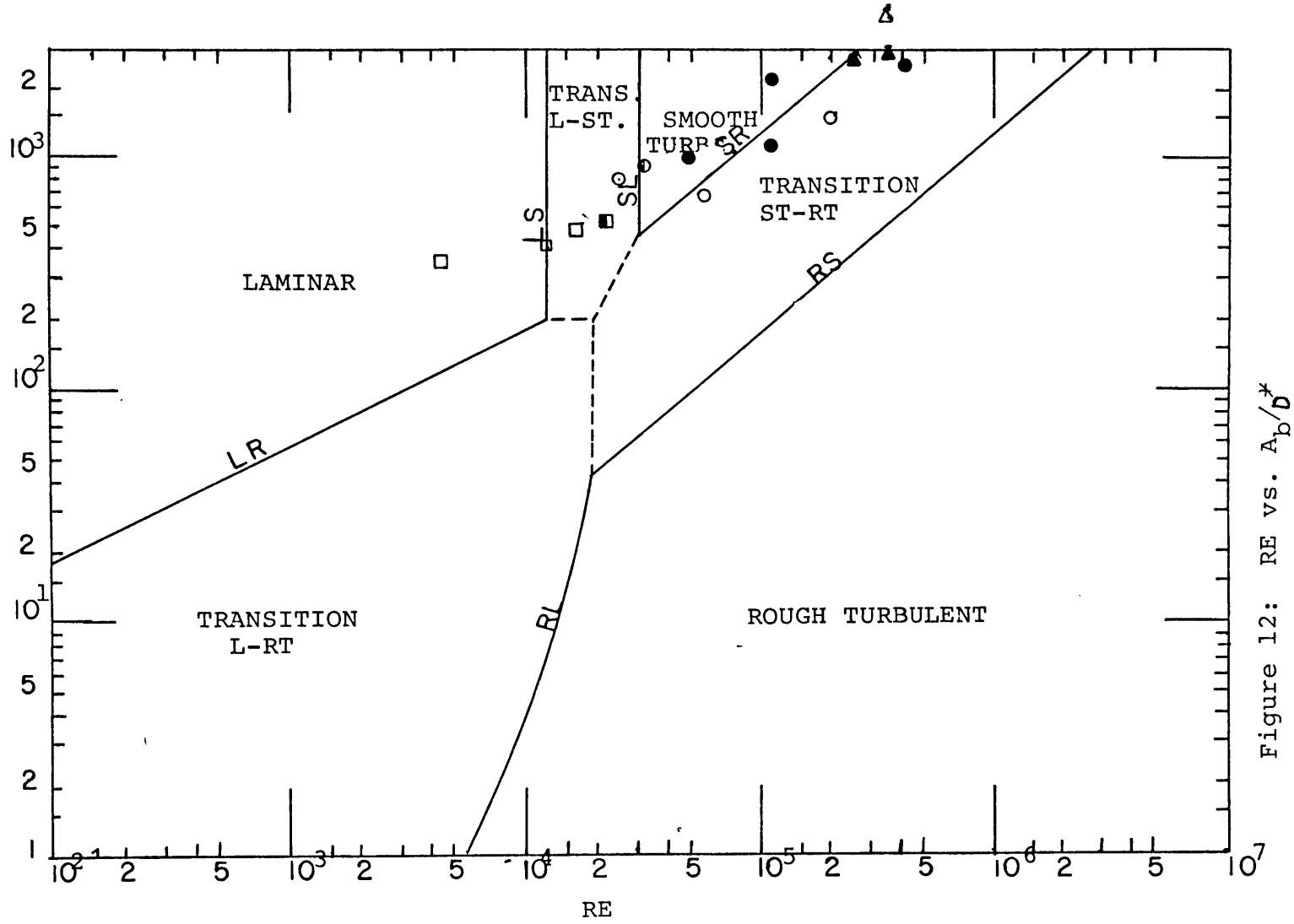

Figure 12: RE vs. A_b/D^*

variable, T, to be small by virtue of Eq.(1).

The ratio a/k_s is all-important at low RE in determining the position of the transition between flow regimes with respect to RE. At the start of a run with an initially planar bed, k_s is best represented by D. The flow environment near the bed and in the boundary layer is dependent on the shear stress, which is described by the ratio a/D. The flow resistance increases as bed forms grow. This increase is related not just to the size of bed forms but to their profile shapes as well. The range of values for k_s cited by Grant and Madsen (1982) reflects the problems involved in determining the flow resistance due to bed forms.

More important to this analysis is the scale of the flow resistance. The flow resistance felt locally at the fluid-solid interface (i.e., the skin friction) is decreased on the average by the presence of bed forms. If U_m is not constrained to be constant, the flow resistance produced by bed forms 2-5 cm high slows the flow well outside the boundary layer. Thus the mean-flow Reynolds number RE represents the diminished U_m established by the bed forms. In this study the effect of flow resistance was not measured but was inherent in any measurements made of U_m. A future study on wave damping could clarify the importance of the different length scales possible for flow resistance. The ratio a/D is most probably the sedimentologically important roughness parameter within the boundary layer.

For rolling-grain ripples the stability of the flow field with respect to a/k_s is all-important. With the preferential transport of grains into low ripples a/k_s decreases within the boundary layer. This lowers the value of RE at which flow becomes rough turbulent. The comparison of run data from this study with Jonsson's boundaries is interesting despite the problems inherent in making such a diagram (Figure 12).

The change in plan shape from 2D to 3D vortex ripples and the change in the pattern of vortexing in the flow indicates different flow environments. In calculating RE for the two bed phases a distinct pattern emerges. According to Jonsson's (1966) diagram, the transition from 2D vortex ripples to 3D vortex ripples at short periods takes the flow from transitional laminar-smooth turbulent into the region of purely smooth turbulent flow. Perhaps flow separation and vortex development occurs with fully smooth turbulent flow for 3D vortex ripples. In watching bed configurations develop during runs, a subtle difference was seen in the vortex action with the two different bed configurations. Conditions that produce 3D vortex ripples contain smaller more rapidly closing vortex cells. The energy of the flow environment is possibly high enough that ripples on the bed incite an irregular vortex pattern.

Analysis of the transition from vortex ripples to nonvortex ripples with respect to RE is interesting. Vortex ripples occur in both the smooth-rough turbulent

transitional and laminar-to-smooth turbulent flow regimes in Jonsson's diagram. All values of RE are at the low end of the range for turbulent flow. As T increases at a given U_m, a/k_s increases linearly. At sufficiently high T the vortex phenomenon occurs in the smooth turbulent transition zone. Once RE is high enough, the flow for the same a/k_s becomes transitional smooth-to-rough turbulent. Reversing-crest ripples occur at the boundary of smooth turbulent flow to smooth-rough turbulent flow. The a/k_s ratio for this boundary is on the order of 500-3000 for the RE conditions produced in the laboratory (taking $k_s=D$) . The T dependence of nonvortex ripples may be attributed to the growth of a/k_s above the level of rough turbulent flow regimes.

The fact that reversing-crest ripples occcur in the transition of rough turbulent flow to rough-smooth turbulent flow in Jonsson's study is interesting. Internal shearing of the fluid is important for dissipating the kinetic energy built up in a half cycle of oscillation. Perhaps the internal shearing of the fluid for flow over reversing-crest ripples does not require vertical velocity fluctuations and thus the flow remains within streamline boundaries. This supposition puts a distinct barrier between the flow phenomenon of vortex-ripple development and reversing-crest ripple or planar-bed development. The high a/k_s ratios of both these flows argues well for the idea of an undisturbed flow within the thick boundary layer anticipated.

The development of nonvortex flow over the sediment bed

may be related to the relative roughness of the bed. The local disruption of flow in the boundary layer is perhaps too small to trigger recirculation. Another possibility is that the velocity supresses vortex formation through much of the flow cycle and then small-scale vortexing occurs after the flow begins to slow and bed forms appear. Nonuniform erosion by vortex action is then precluded by the high velocity of the return flow eroding the ripple crests. The flow is less affected by the bed configuration in the reversing-crest region of U_m and T space.

The transition from vortex-ripple beds to planar beds is interesting in terms of the values of RE for the flow conditions. For vortex-ripple flows and reversing-crest-ripple flows the value of RE lies near the transition from smooth-to-rough turbulent flow to smooth turbulent flow. Planar-bed flows in this study have RE values that fall in the region of smooth turbulent flow. This occurs at RE values similar to those for vortex-ripple flows but at higher a/k_s ratios (i.e. longer-period flows). This implies a negative slope for the boundary zone betweeen the two phenomena; the steepness of this boundary is unknown. It should be noted that conditions of plane-bed flow for low T were unattainable with the experimental arrangement used. A future study capable of high U_m at low T would permit examination of this predicted slope.

CONCLUSIONS

The four dimensionless parameters used in this study add a helpful perspective on the stability of sedimentary bed forms under different flow conditions. Values of U_m and T for ripple growth and development are directly dependent on D. When one of the parameters, ρ_s/ρ, is constant, U_m and T increase simultaneously along the curve for the threshold of sediment movement in oscillatory flows. The curve is reasonably well predicted by empirical equations relating shear stress to bed roughness. 2D vortex ripples are the dominant bed form in fine to medium sands under the range of natural flow conditions. Reversing-crest ripples are a large U_m and T phenomenon with an asymmetrical vertical profile. Rolling-grain ripples are stable at conditions of very low U_m and T in fine sand. At very large U_m the sediment bed contains no small-scale bed forms. Irregular vortex ripples are stable in high-energy flows with more rapid accelerations and decelerations than 2D vortex-ripple flows. There is a distinct overlap region between vortex ripples and reversing-crest ripples at high T for vortex-ripple stability and it has a strong dependence on D.

The questions put forth in the study pertaining to bed-phase stability and the transitions between different bed forms have been partially addressed and answered, but much work remains to be done. 2D vortex ripples are stable as flow conditions pass down through the sediment movement boundary. The transition from 2D vortex ripples to 3D

vortex ripples is a broad zone of U_m and T conditions for a given D. 2D and 3D bed configurations can occur together or separately over this zone. The development of 3D vortex ripples from 2D vortex ripples involves a change in the shape and orientation of vortex axes from horizontal linear to 3D, resulting in nonuniform erosion in both streamwise and cross-stream directions. Reversing-crest ripples develop without being associated with prominent vortices. The transition to planar beds from rippled beds is gradual, with a decrease in ripple height near the boundary. Planar-bed flows have a uniform erosion pattern, while vortex-ripple flows do not. Hysteresis effects are not important in oscillatory flow; rolling-grain ripples develop and stabilize in a distinct and unique range of flow conditions.

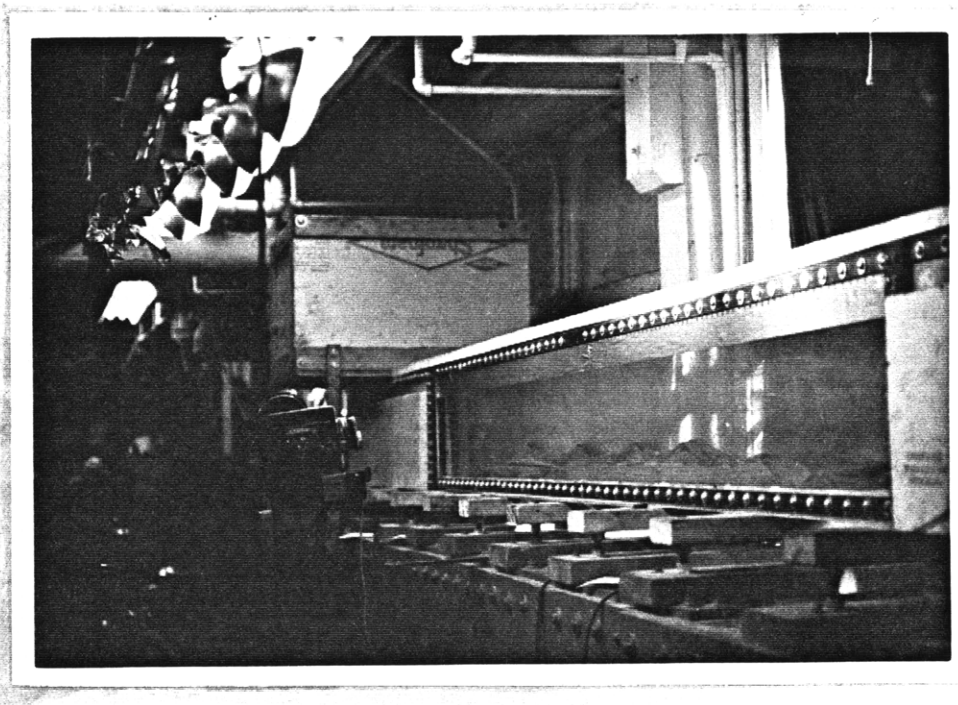

Figure 13: Experimental duct and photo set-up.

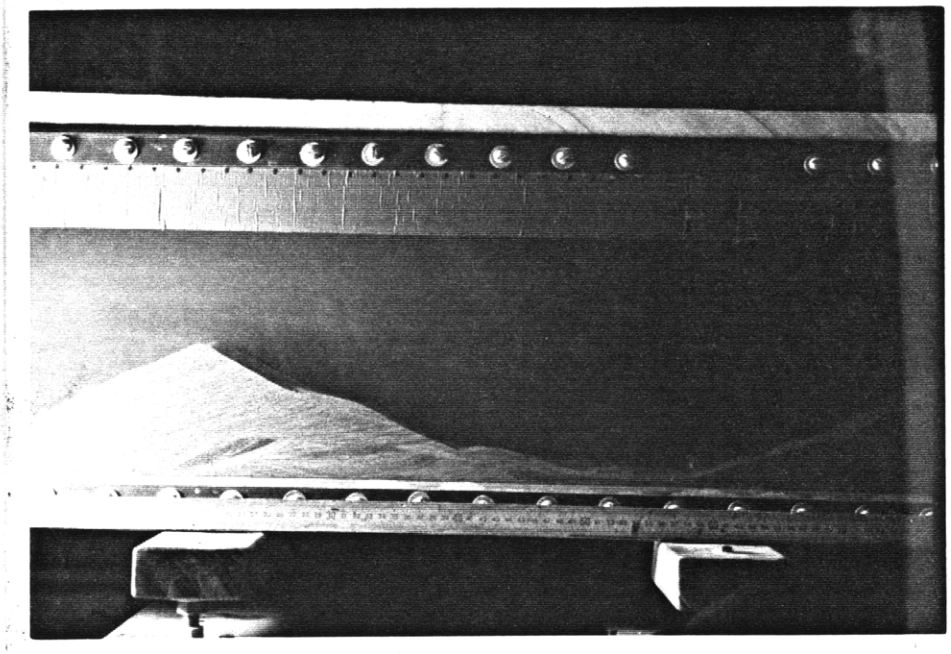

Figure 14: Run 16 coarser sand, unidirectional ripples on vortex-ripple shoulders (Tables 1 an 3).

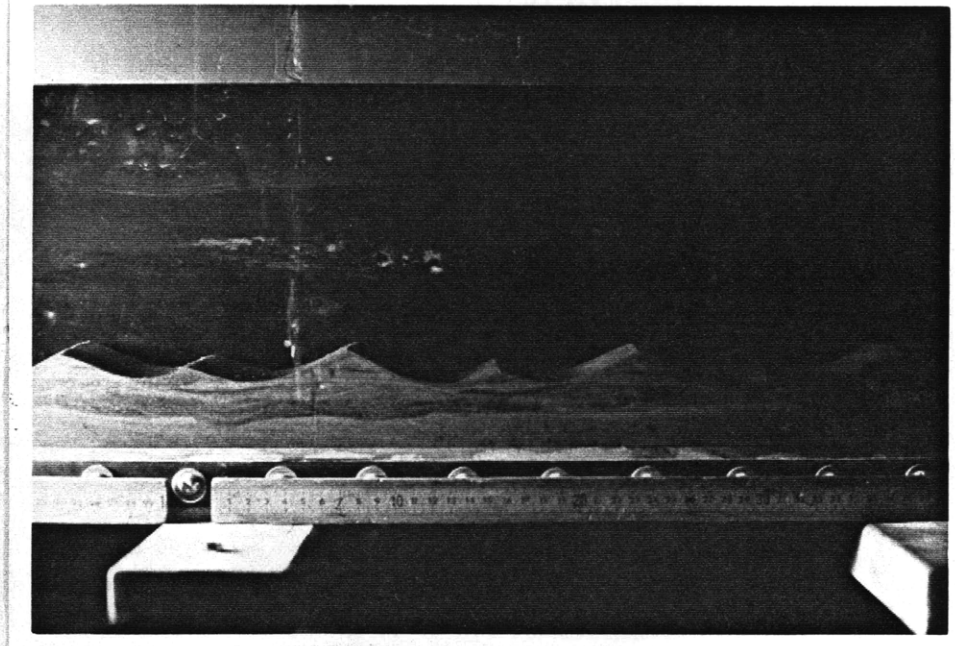

Figure 15: Run 11 coarser sand, 2D vortex ripples with trough ripples.

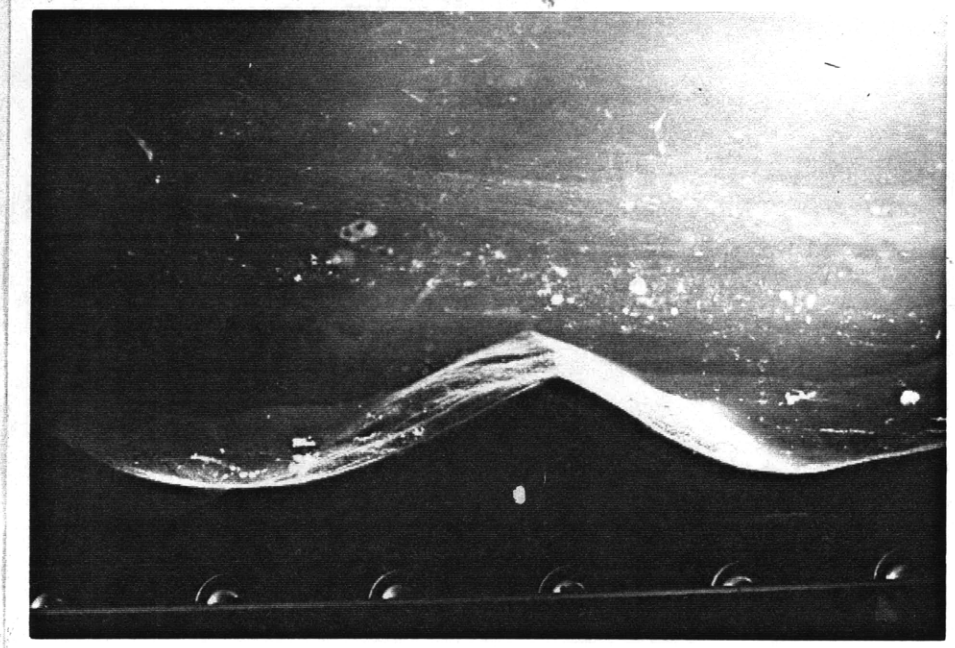

Figure 16: Run 10 coarser sand, 2D vortex ripples with convex shoulders

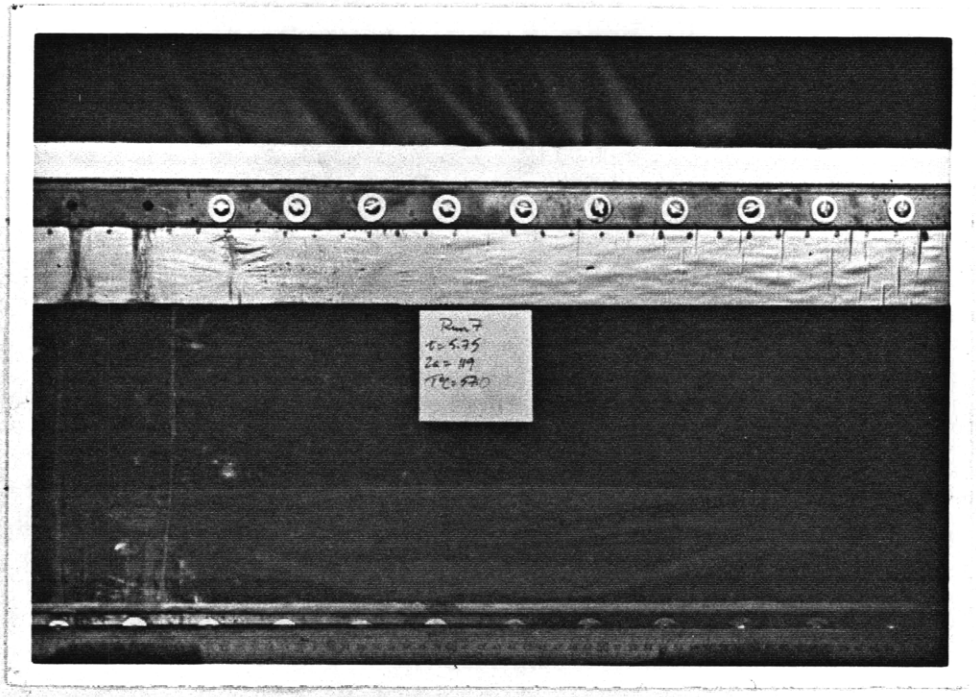

Figure 17: Run 7 finer sand planar bed (Tables 2 and 4)

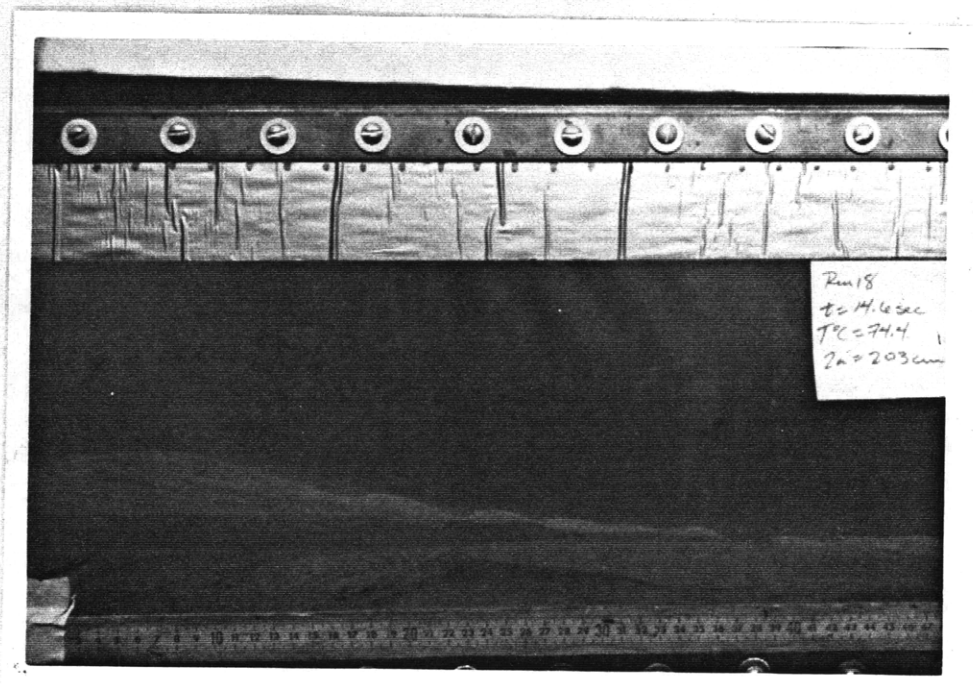

Figure 18: Run 18 finer sand, reversing crest on vortex ripples.

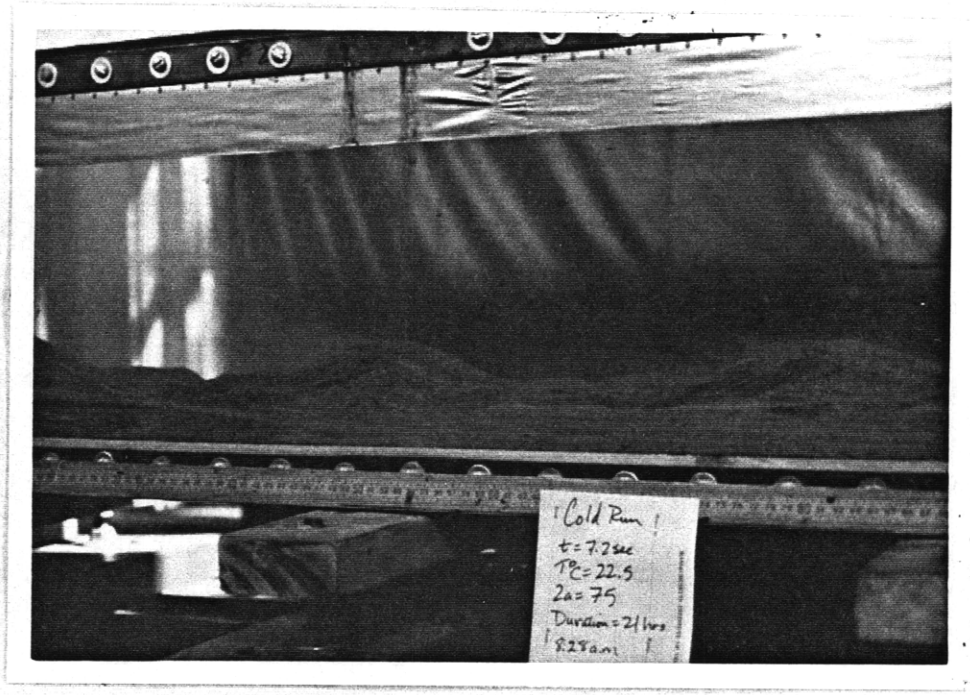

Figure 19: ST1, cold run (Tables 1 and 3)
2D vortex ripples.

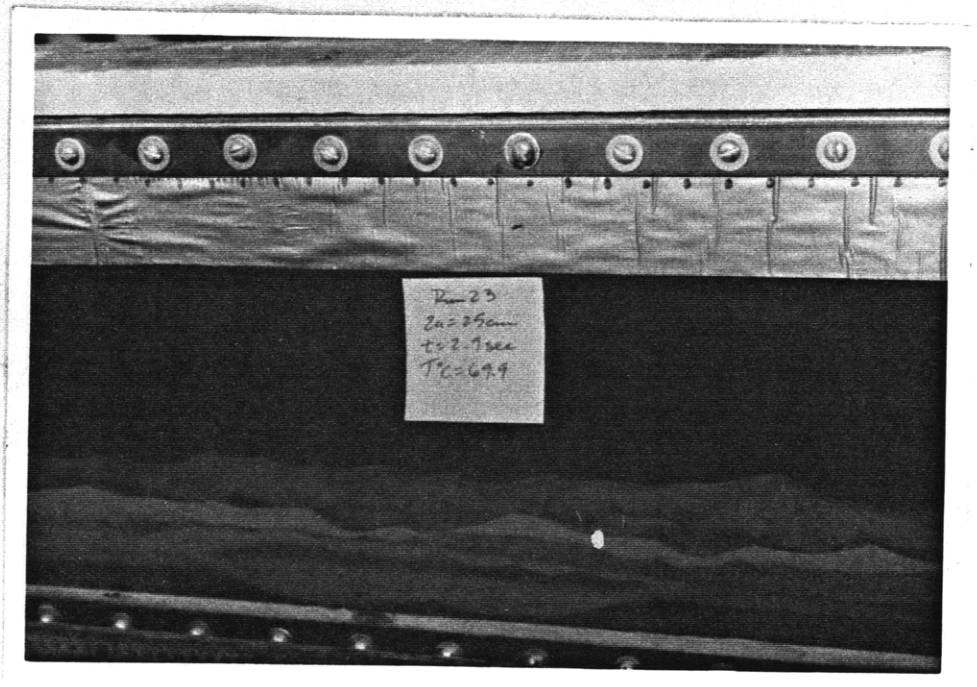

Figure 20: Run 23 finer sand, 3D vortex ripples.

Table 1: 0.15 mm sand runs in this study.

RUN	° C	2a	$\bar{U}$ cm/sec	U_m cm/sec	T sec	λ cm	h cm	Bed
1	51.0	81.0	34.46	54.14	4.7	33.0	3.7	3D
2	56.5	39.5	16.80	26.40	4.7	18.25	2.9	2D
3	56.0	39.5	16.81	26.40	4.7	23.0	3.3	2D
4	59.0	13.5	9.64	15.14	2.8	11.5	2.1	2D
5	50.0	20.5	15.00	23.56	2.8	12.5	2.3	2D
6	60.5	23.5	17.28	27.14	2.72	13.2	2.2	2D
7	64.5	43.5	22.59	35.50	3.85	25.3	3.2	2D
8	60.5	38.5	20.10	31.58	3.83	20.3	4.0	2D
9	58.7	33.5	17.49	27.47	3.83	18.5	3.32	2D
10	63.5	27.8	14.52	22.8	3.83	16.3	2.84	2D
11	60.0	20.3	10.57	16.60	3.85	11.5	1.83	2D
12	65.0	31.0	10.44	16.40	5.94	17.2	2.76	2D
13	62.5	51.0	26.5	41.61	3.85	22.2	4.1	2D
14	61.5	10.5	5.45	8.57	3.85	1.6	0.2	RGR
15	61.5	16.0	6.80	10.69	4.7	---	---	NM
16	62.0	105.5	19.36	30.41	10.9	56.0	10.3	2D
17	64.5	30.0	21.43	33.66	2.8	17.0	2.45	3D
18	70.0	48.0	24.80	38.96	3.87	20.4	3.98	2D
19	59.5	37.5	26.8	42.1	2.8	20.0	1.90	3D
20	68.5	78.8	29.7	46.8	5.3	33.0	3.9	2D
21	64.2	72.0	27.2	42.8	5.3	30.5	4.4	2D
22	64.2	55.9	21.1	33.2	5.3	27.0	3.8	2D
23	67.1	52.5	19.8	31.2	5.3	24.0	4.8	2D
24	69.7	35.3	13.9	21.0	5.3	20.2	3.4	2D
25	75.5	19.5	7.4	11.6	5.3	18.8	3.1	2D
26	63.0	18.3	6.9	10.9	5.3	4.0	0.3	RGR

Table 1 (continued)

RUN	° C	2a	$\bar{\bar{U}}$ cm/sec	Umcm/sec	T sec	λ cm	h cm	Bed
26b	63.0	18.3	6.9	10.9	5.3	9.4	1.4	2D
27a	63.0	25.2	9.5	15.0	5.3	9.3	1.7	2D
27b	63.0	23.0	8.7	13.66	5.30	13.8	2.6	2D
28	62.0	12.5		10.19	3.85	---	---	NM
29	62.0	24.1		12.75	5.94	---	---	NM
30	62.0	170.7		49.2	10.9	72.5	11.1	2D/3D
31	62.0	62.0		50.6	3.85	---	---	2D
32	62.0	47.5		38.75	3.85	---	---	2D/3D
ST 1	21.9	75.5	21.0	32.9	7.2	29.7	4.0	2D
ST 2	22.0	42.0	18.3	28.68	4.6	17.3	2.8	2D

Table 2: 0.09 mm sand runs form this study.

RUN	° C	2a	$\overline{\overline{U}}$ cm/sec	Umcm/sec	T sec	λ cm	h cm	Bed
1	65.2	22.0	7.6	12.0	5.75	11.6	1.45	2D
2	65.2	40.7	14.0	22.2	5.75	---	---	3D
3	72.5	59.6	20.6	32.6	5.75	3.6	0.5	RC
4a	60.2	78.0	26.9	42.6	5.75	4.6	.6	RC
4b	60.2	78.0	26.9	42.6	5.75	55.0	3.5	2D
5a	61.0	93.5	32.2	51.1	5.75	64.5	6.7	2D
5b	61.0	93.5	32.2	51.1	5.75	5.0	0.8	RC
6	67.5	105.5	36.45	57.0	5.75	70.0	8.2	2D
7	57.0	119.0	41.00	65.0	5.75	---	---	PLANAR
8	57.0	130.0	44.8	71.0	5.75	---	---	PLANAR
9	48.4	161.0	42.9	67.4	7.5	---	---	PLANAR
10	64.0	29.0	9.70	15.2	6.0	12.42	1.8	2D
11a	64.0	48.0	12.3	19.3	7.8	18.6	1.9	RC
11b	64.0	48.0	12.3	19.3	7.8	4.0	0.8	TR
12	62.8	104.5	20.9	32.8	10.0	3.6	0.3	RC
13	64.0	48.0	12.3	19.3	7.8	4.0	0.8	RC
14	60.3	81.5	20.9	32.8	7.8	3.9	0.4	RC
15a	61.0	112.0	28.7	45.1	7.8	99.0	7.6	2D
15b	61.0	112.0	28.7	45.1	7.8	6.0	0.4	RC
16a	61.0	135.0	34.6	54.4	7.8	---	---	VORTEX
16b	61.0	135.0	34.6	54.4	7.8	5.6	0.35	RC
17	51.4	167.0	33.4	52.5	10.0	---	---	VORTEX
18a	48.8	203.0	27.8	43.68	14.6	110.0	6.8	2D
18b	48.8	203.0	27.8	43.68	14.6	7.75	0.8	RC
19	61.2	6.5	4.5	7.0	2.9	---	---	PB
20	61.0	15.0	10.3	16.2	2.9	?	?	2D

Table 2 (continued)

RUN	° C	2a	$\overline{\overline{U}}$ cm/sec	Umcm/sec	T sec	λ cm	h cm	Bed
21	59.6	17.0	11.7	18.4	2.9	11.0	2.1	2D/3D
22	59.6	21.0	14.5	22.7	2.9	10.6	1.3	3D
23	69.9	25.0	17.2	27.1	2.9	----	---	3D
24	67.2	33.0	22.8	35.7	2.9	21.0	---	3D
25	67.2	39.0	26.9	42.2	2.9	6.5	2.0	3D
26	52.3	15.5	13.5	21.2	2.3	6.6	1.2	2D/3D
27	62.2	16.0	13.9	21.9	2.3	7.6	1.4	2D
28	54.0	22.5	19.6	30.7	2.3	8.0	1.2	3D
29	52.4	18.0	15.7	24.6	2.3	7.5	1.2	2D/3D
30	69.0	40.5	14.7	23.1	5.5	21.2	1.8	2D
31a	65.2	51.0	18.5	29.1	5.5	75.0	4.1	VORTEX
31b	65.2	51.0	18.5	29.1	5.5	3.25	0.7	RC
32-ST1	65.0	42.0	15.3	24.0	5.5	15.6	2.1	2D
33	65.0	26.0	11.6	18.2	4.5	14.0	2.0	2D
34a	65.0	35.0	15.6	24.4	4.5	18.0	2.7	3D
34b	65.0	25.0	15.6	24.4	4.5	3.5	0.5	RC
35-ST2	64.4	21.0	13.1	20.9	3.15	10.5	1.5	2D
36	60.0	29.0	18.1	28.9	3.15	8.33	2.3	2D/3D

Table 3: Scaled data from 0.15 mm sand runs.

RUN	D* mm	2a*	U_m* cm/sec	T* sec	λ* cm	h* cm	λ/h	Bedform
1	0.268	145.7	72.20	6.34	59.2	6.64	8.92	3D
2	0.284	74.9	36.20	6.50	34.7	5.52	6.29	2D
3	0.282	74.94	36.11	6.52	43.5	6.24	6.97	2D
4	0.291	26.3	20.97	3.94	22.4	4.10	5.46	2D
5	0.265	37.24	31.20	3.75	22.2	4.08	5.44	2D
6	0.295	45.19	37.86	3.85	26.1	4.35	6.00	2D
7	0.307	89.41	50.43	5.57	52.0	6.64	7.84	2D
8	0.295	76.15	44.06	5.43	39.8	7.92	5.04	2D
9	0.290	65.08	38.00	5.38	36.0	6.45	5.58	2D
10	0.304	56.67	32.24	5.52	33.2	5.78	5.75	2D
11	0.294	40.02	23.11	5.44	22.65	3.60	6.29	2D
12	0.308	64.09	23.35	8.62	35.6	5.71	6.23	2D
13	0.301	102.93	58.58	5.52	44.8	8.27	5.42	2D
14	0.298	20.99	12.01	5.49	3.2	0.40	7.99	RGR
15	0.298	31.95	14.98	6.70	---	---	---	NM
16	0.299	211.86	42.72	15.58	112.5	20.69	5.44	2D
17	0.307	61.65	47.82	4.05	35.0	5.04	6.94	3D
18	0.322	103.90	56.67	5.76	44.1	8.61	5.13	2D
19	0.292	73.5	58.5	3.95	39.2	3.72	10.52	3D
20	0.318	168.3	67.7	7.82	70.5	8.33	8.46	2D
21	0.306	147.7	60.72	7.70	62.6	9.03	6.93	2D
22	0.306	114.7	47.1	7.70	55.4	7.80	7.10	2D
23	0.315	111.0	45.1	7.70	50.8	10.21	4.95	2D
24	0.321	76.15	30.5	7.91	43.6	7.32	5.91	2D
25	0.338	44.25	17.3	8.12	42.7	7.04	6.00	2D
26a	0.302	37.1	15.4	7.60	8.1	0.61	13.3	RGR
26b	0.302	37.1	15.4	7.60	19.1	2.84	6.64	2D

Table 3 (continued)

RUN	D* mm	2a*	U_m* cm/sec	T* sec	λ* cm	h* cm	λ/h	Bedform
27a	0.302	51.1	21.2	7.6	18.9	3.45	5.4	2D
27b	0.302	46.7	19.3	7.6	28.0	5.27	5.3	2D
28	0.299	25.1	14.3	5.5	---	---	---	NM
29	0.299	48.4	17.9	8.5	---	---	---	NM
30	0.299	342.9	69.1	15.6	145.64	22.3	6.53	2D
31	0.299	124.5	71.1	5.5	---	---	---	2D
32	0.299	95.4	54.4	5.5	---	---	---	2D
ST1	0.183	92.6	36.4	8.0	36.45	4.91	7.42	2D
ST2	0.183	51.6	31.8	5.1	21.27	3.44	6.18	2D

Table 4: Scaled data from 0.09 mm sand runs.

RUN	D* mm	2a*	U_m* cm/sec	T* sec	λ* cm	h* cm	λ/h	Bedform
1	0.182	45.6	17.1	8.4	24.0	3.0	8.0	2D
2	0.182	84.3	31.6	8.4	---	---	---	3D
3	0.195	131.9	47.9	8.7	8.1	1.1	7.2	RC
4a	0.174	154.0	59.4	8.1	9.1	1.2	7.6	RC
4b	0.174	154.0	59.4	8.1	108.6	6.9	15.7	2D
5a	0.175	186.0	71.5	8.2	128.3	13.3	9.6	2D
5b	0.175	186.0	71.5	8.2	9.9	1.6	6.3	RC
6	0.186	223.2	82.0	8.4	148.0	17.3	8.5	2D
7	0.168	227.5	89.2	8.0	---	---	---	VORTEX
8	0.168	248.5	97.5	8.0	---	---	---	PB
9	0.154	281.1	88.6	10.0	---	---	---	PB
10	0.180	59.4	21.5	8.7	25.4	3.7	6.9	2D
11a	0.180	98.3	27.4	11.3	38.1	3.9	9.8	RC
11b	0.180	98.3	27.4	11.3	8.2	1.6	5.0	TR
12	0.178	211.4	46.2	14.4	7.3	0.6	12.0	RC
13	0.180	98.3	27.4	11.3	38.1	3.9	9.8	RC
14	0.174	161.1	45.7	11.1	7.7	0.8	9.7	RC
15a	0.175	222.8	63.1	11.1	197.0	15.1	13.0	2D
15b	0.175	222.8	63.1	11.1	11.9	0.8	15.0	RC
16a	0.175	268.6	76.1	11.1	---	---	---	2D
16b	0.175	268.6	76.1	11.1	11.1	0.7	16.0	RC
17	0.159	301.0	70.0	13.5	---	---	---	PB
18a	0.154	355.5	57.5	19.4	192.6	11.9	16.2	2D
18b	0.154	355.5	57.5	19.4	13.6	1.4	9.7	RC
19	0.175	13.0	9.8	4.1	---	---	---	NM
20	0.175	29.8	22.7	4.1	?	?		2D
21	0.173	33.4	25.6	4.1	21.6	4.1	5.2	2D/3D

Table 4 (continued)

RUN	D*mm	2a*	U_m*cm/sec	T*sec	λ*cm	h*cm	λ/h	Bedform
22	0.173	41.2	31.5	4.1	20.8	2.6	8.15	3D
23	0.190	54.0	39.4	4.3	---	---	---	3D
24	0.186	69.6	51.3	4.3	44.3	---	---	3D
25	0.186	82.3	60.7	4.3	13.7	4.2	3.25	3D
26	0.160	28.2	28.4	3.1	12.0	2.2	5.50	2D/3D
27	0.177	32.2	30.8	3.3	15.3	2.8	5.44	2D
28	0.163	41.7	41.5	3.2	14.8	4.3	6.66	3D
29	0.160	32.8	33.0	3.1	13.7	2.2	6.25	2D/3D
30	0.188	86.9	33.5	8.1	45.5	3.9	11.78	2D
31a	0.182	105.6	41.5	8.0	155.3	8.5	18.3	VORTEX
31b	0.182	105.6	41.5	8.0	6.73	1.45	4.64	RC
32-ST1	0.182	86.8	34.2	8.0	32.2	4.3	7.43	2D
33	0.182	53.7	25.9	6.5	28.9	4.1	7.00	2D
34a	0.182	72.4	34.7	6.5	37.2	5.6	6.67	3D
34b	0.182	72.4	34.7	6.5	7.2	1.0	7.00	RC
35-ST2	0.181	43.2	29.7	4.6	21.6	3.1	7.00	2D
36	0.173	57.1	40.2	4.6	16.4	4.5	3.62	2D/3D

Table 5: Scaled data from Lofquist (1979).

RUN	D* mm	2a*	U_m* cm/sec	T* sec	λ* cm	h* cm	λ/h	Bedform
1	0.68		38.47	9.24	89.92	19.2	4.68	2D
2	0.68		39.58	9.00	72.22	15.28	4.73	2D
3-6	0.68		31.24	12.36	68.14	13.5	5.05	2D
7	0.68		39.25	7.26	68.38	12.44	5.5	2D
8	0.68		48.25	5.91	52.9	11.02	4.8	2D
9	0.68		60.49	4.71	49.56	9.34	5.31	2D
11	0.68		38.47	4.64	34.44	6.67	5.7	2D
13-18	0.68		40.25	5.81	40.39	8.09	4.99	2D
19	0.68		32.02	8.91	61.95	13.11	4.73	2D
23-25	0.68		39.47	3.79	30.73	5.3	5.79	2D
26	0.68		34.58	3.13	29.49	4.266	6.92	2D
28	0.68		34.47	3.41	28.37	4.36	6.51	2D
30-32	0.68		35.58	3.01	25.77	4.01	6.42	2D
33-36	0.68		36.03	3.08	23.54	4.2	5.6	2D
37	0.68		38.36	4.97	39.40	7.48	5.36	2D
48	0.68		36.80	2.52	13.50	3.51	5.97	2D
49	0.68		38.36	4.82	31.47	6.81	4.62	2D
51	0.68		37.36	3.81	33.82	5.12	6.61	2D
52-54	0.68		43.36	4.95	41.63	8.42	5.09	2D
55	0.68		85.62	2.50	32.46	5.61	5.78	2D
56-57	0.68		35.47	3.01	27.01	4.22	6.42	2D
58	0.68		37.02	5.77	3D	---	---	3D
59	0.68		29.13	3.67	19.82	2.69	7.37	2D/3D
60	0.68		20.68	5.16	19.82	2.48	8.00	2D
61	0.68		31.69	3.38	3D	---	---	3D
62	0.68		37.58	9.48	3D	---	---	3D
63	0.68		19.90	17.86	3D	---	---	3D

Table 5 (continued)

RUN	D*mm	2a*	U_m*cm/sec	T*sec	λ*cm	h*cm	λ/h	Bedform
65	.223		29.13	12.25	3D	---	---	3D
66	.223		37.47	9.5	3D	---	---	3D
68	.223		26.91	3.31	17.34	2.48	7.00	2D/3D
69	.223		24.35	3.65	17.34	2.14	8.44	2D
70	.223		29.58	3.01	16.48	2.21	7.47	3D
71	.223		31.13	2.85	3D	---	---	3D
72-77	.223		23.68	3.05	14.12	2.02	6.99	2D
78	.223		31.02	4.59	3D	---	---	3D
80-81	.223		23.34	6.11	26.07	3.46	7.52	2D
82	.223		25.35	8.45	33.2	4.09	8.12	2D
83	.223		31.8	6.72	3D	---	---	3D
84	.223		31.24	2.85	3D	---	---	3D

Table 6: Scaled data from Mogridge & Kamphuis (1972)

RUN	D* mm	2a*	U_m* cm/sec	T* sec	λ* cm	h* cm	λ/h	° C
1	.381	5.29	14.89	1.12	3.53	.60	5.91	13.61
2	.379	5.66	15.98	1.11	3.80	.56	6.71	13.33
4	.387	6.44	17.99	1.12	4.02	.57	6.95	14.44
5	.387	6.93	19.38	1.12	4.32	.69	7.14	14.44
6	.379	7.15	20.18	1.11	4.43	.68	6.56	13.33
7	.379	7.71	21.78	1.11	5.05	.70	7.19	13.3
8	.383	6.67	18.73	1.12	4.68	.65	7.16	13.8
9	.340	5.49	16.37	1.05	3.41	.48	7.05	7.5
10	.328	5.96	18.07	1.04	3.90	.56	6.96	5.8
11	.338	5.51	16.46	1.05	3.58	.50	7.10	7.2
12	.321	4.89	14.99	1.02	2.99	.39	7.71	4.7
13	.319	5.85	18.02	1.02	3.79	.55	6.96	4.4
14	.327	5.44	16.55	1.03	3.26	.49	6.70	5.6
15	.343	7.58	22.48	1.04	4.70	.66	7.11	8.1
16	.328	7.34	22.25	1.04	4.79	.68	7.07	5.8
17	.342	7.93	23.58	1.06	4.79	.66	7.30	7.8
18	.325	6.34	19.32	1.03	4.10	.55	7.38	5.3
19	.328	7.80	23.67	1.04	4.55	.61	7.50	5.8
20	.328	7.10	21.54	1.04	4.58	.59	7.80	5.8
44	.403	5.87	17.36		3.61	.54	6.63	16.7
45	.412	5.16	15.08	1.07	3.48	.50	7.0	18.1
46	.417	6.56	19.07	1.08	4.66	.62	6.7	18.9
47	.420	8.42	24.38	1.08	5.25	.72	7.3	19.2
48	.421	7.34	21.22	1.09	4.73	.66	7.2	19.4
49	.410	7.52	22.06	1.07	4.72	.64	7.36	17.8
50	.415	6.66	19.35	1.08	4.23	.62	6.81	18.6
51	.418	7.52	21.82	1.08	4.92	.66	7.55	18.9
52	.420	8.53	24.73	1.08	5.31	.72	7.42	19.2
53	.420	7.56	17.50	1.36	5.20	.78	6.69	19.2
54	.417	9.26	21.53	1.35	6.06	.81	7.29	18.9
55	.420	8.33	19.30	1.36	5.62	.81	6.96	19.2
56	.416	8.81	20.51	1.35	5.91	.92	6.45	18.6
57	.413	6.71	15.65	1.35	4.03	.61	6.52	18.3
58	.416	7.04	16.38	1.35	4.82	.68	7.09	18.6
59	.416	6.86	15.96	1.35	4.78	.68	7.04	18.6
60	.416	12.88	15.01	2.70	7.60	1.33	5.7	18.6
61	.420	20.49	23.73	2.71	9.02	1.32	6.9	19.2
62	.420	13.73	15.91	2.71	8.12	1.53	5.3	19.2
63	.420	12.95	15.01	2.71	7.70	1.16	6.62	19.2
64	.410	12.46	18.16	2.16	7.33	1.08	6.78	17.8
65	.420	11.46	16.51	2.18	7.17	.99	7.27	19.2
73	.438	7.76	20.37	1.20	4.64	.71	6.48	21.9
74	.438	6.82	17.91	1.20	4.15	.63	6.65	21.9
75	.438	9.16	24.02	1.20	5.64	.85	6.70	21.7
76	.438	9.45	24.78	1.20	6.05	.91	6.69	21.9
77	.440	8.51	22.13	1.20	5.27	.79	6.72	22.2
78	.442	9.91	25.88	1.20	6.05	.88	6.86	22.5
79	.437	7.55	19.83	1.20	4.44	.71	6.22	21.7
80	.437	6.52	17.15	1.20	4.26	.59	7.21	21.7
81	.437	9.45	24.82	1.20	5.81	.81	7.19	21.7
185	.410	176.68	64.71	8.58	48.61	7.96	6.10	17.8
163	.406	21.23	25.01	2.67	14.59	2.37	6.16	17.2
164	.406	35.41	26.07	4.27	22.24	3.75	5.92	17.2

Table 6 (continued)

RUN	D*mm	2a*	U_m*cm/sec	T*sec	λ*cm	h*cm	λ/h	° C
165	.410	35.48	25.99	4.29	22.81	3.85	5.92	17.8
166	.410	58.84	43.10	4.29	32.00	5.49	5.84	17.8
167	.410	49.77	25.86	6.05	32.36	5.51	5.87	17.8
168	.410	66.93	34.77	6.05	42.91	6.59	6.51	17.8
169	.410	72.96	53.44	4.29	38.54	5.80	6.64	17.8
170	.410	81.95	30.01	8.58	50.47	7.79	6.48	17.8
171	.410	97.47	35.69	8.58	56.89	10.04	5.67	17.8
172	.410	118.24	43.31	8.582	62.40	10.85	5.75	17.8
173	.410	122.38	35.85	10.72	68.41	11.52	5.94	17.8
174	.410	138.73	33.87	12.87	74.05	11.82	6.27	17.8
175	.410	152.12	37.14	12.87	83.68	13.07	6.40	17.8
176	.413	173.09	36.07	15.08	93.14	15.59	5.97	18.3
177	.413	213.43	44.48	15.08	116.68	21.13	5.52	18.3
178	.410	30.69	22.48	4.29	19.55	3.39	5.78	17.8
179	.410	47.99	35.16	4.29	28.24	4.38	6.45	17.8
180	.410	67.63	49.53	4.29	37.58	5.19	7.24	17.8
181	.410	86.62	63.45	4.29	31.62	5.63	5.62	17.8
182	.410	99.99	73.24	4.29	25.82	4.41	5.86	17.8

Table 7: Scaled data from Kennedy and Falcon (1965)

RUN	D^* mm	$2a^*$	$U_m{}^*$ cm/sec	T^* sec	λ^* cm	h^* cm	λ/h	Bedform
23	0.41	12.3	25.4	1.6	8.0	1.32		2D
22a	0.41	13.5	23.9	1.8	9.1	1.48		2D
22b	0.41	16.2	29.1	1.8	10.8	2.05		2D
20	0.41	12.0	24.3	1.6	7.8	1.48		2D
19	0.41	10.8	19.2	1.8	7.5	1.61		2D
17	0.41	8.1	16.4	1.6	5.8	0.90		2D
15	0.12	5.0	13.7	1.2	3.9	0.64		2D
13b	0.12	15.1	14.0	2.2	6.0	1.04		2D
13a	0.12	13.5	19.6	2.2	7.1	1.41		2D
2	0.12	14.7	17.4	2.6	6.9	1.25		2D

Table 8: Scaled data from Carstens et al.(1969)

RUN	D* mm	2a*	U_m* cm/sec	T* sec	λ* cm	° C	λ/h	Bedform
106	0.249		36.6	4.1	14.2	26.2	7.46	2D
85	0.216		16.7	3.9	13.2	17.2	5.52	2D
96A	0.246		23.6	4.1	19.6	25.3	6.21	2D
111A	0.244		47.6	4.0	13.6	24.8	8.00	2D
112B	0.241		62.6	4.0	12.7	23.9	20.83	?
114A	0.242		16.4	4.0	13.3	24.4	5.03	2D
21	0.388	23.2	17.9	4.1	13.8	26.1	5.85	2D
22	0.379	30.6	19.7	4.0	16.2	24.4	5.71	2D
23	0.376	34.6	27.2	4.0	18.4	23.9	5.68	2D
24	0.382	39.5	30.7	4.0	18.7	25.0	5.59	2D
25	0.370	51.9	41.1	4.0	24.2	22.8	5.88	2D
26	0.370	58.3	46.1	4.0	27.5	22.8	6.17	2D
27	0.370	65.0	51.8	3.9	30.5	22.8	7.58	2D
29B	0.370	80.7	64.0	4.0	33.6	22.8	8.70	2D
30B	0.366	87.8	70.5	3.9	24.8	22.2	9.43	2D
31B	0.366	109.8	88.1	3.9	23.6	22.2	38.46	?
32B	0.362	95.1	76.5	3.9	26.8	21.4	15.38	?
36	0.370	69.9	55.4	4.0	30.5	22.8	7.63	2D
51	0.376	20.3	15.7	4.0	13.2	23.9	5.46	2D
52	0.376	21.9	17.1	3.9	13.8	23.9	6.37	2D
53	0.373	18.4	15.6	3.7	1.0	23.3	5.68	2D
54	0.370	23.8	18.2	4.1	14.7	22.8	5.71	2D
55	0.378	19.7	14.4	4.3	13.4	24.2	5.88	2D
63	0.762	26.3	20.3	4.1	19.1	25.8	5.24	2D
64	0.760	31.2	24.1	4.1	21.7	25.6	5.13	2D
65A	0.746	35.1	27.5	4.0	23.1	24.4	5.38	2D
66	0.741	40.7	31.9	4.0	25.8	23.9	5.18	2D
67	0.753	47.7	37.3	4.0	30.7	25.0	5.26	2D
68	0.746	50.1	39.0	4.0	32.1	24.4	5.38	2D
69	0.753	57.5	44.8	4.0	37.4	25.0	5.00	2D
70	0.753	62.3	48.6	4.0	33.1	25.0	5.41	2D
71	0.753	63.8	49.7	4.0	34.0	25.0	5.41	2D
72	0.753	68.5	53.7	4.0	38.6	25.0	5.35	2D
73	0.728	72.4	57.4	4.0	32.6	22.8	5.21	2D
74	0.728	76.7	60.5	4.0	37.8	22.8	5.08	2D
75	0.728	81.3	64.3	4.0	48.7	22.8	6.67	2D
76	0.728	87.6	69.8	3.9	47.0	22.8	5.52	2D
77	0.728	93.2	73.9	4.0	44.5	22.8	5.78	2D
78	0.728	97.6	79.0	3.9	57.7	22.8	6.76	2D
79	0.734	106.3	83.7	4.0	55.3	23.3	6.37	2D
80A	0.728	31.0	24.6	4.0	21.6	22.8	5.56	2D

REFERENCES

Allen, J. R. L., 1980, Sand waves: A model of origin and internal structure: Sed. Geol., v. 26, p. 281-328.

_____, 1968, Current ripples; their relation to patterns of water and sediment motion: North-Holland Pub. Co., Amsterdam, 433 p.

Bagnold, R.A., 1946, Motion of Waves in Shallow Water, Interaction Between Waves and Sand Bottoms: Proceedings, Royal Society of London, Series A, v. 187, p.1-18.

Carstens, M.R., Neilson, F. M., and Altinbilek, H. D., 1969, Bed Forms Generated in the Laboratory Under an Oscillatory Flow: TM-28, U.S. Army Corps of Engineers, Coastal Engineering Research Center, Washington, D.C.

Clifton, H. E., 1975, Wave-Formed Sedimentary Structures-A Conceptual Model: ?

Clifton, H. E., Hunter, R. E., and Phillips, R.L., 1971, Depositional structures and processes in the non-barred high energy nearshore: Jour. Sed. Petrology, v. 41, p.651-670.

Davidson-Arnott, R.G.D., and Greenwood, B., 1974, Bedforms and structures associated with in the shallow-water wave environment, Kouchibouguac Bay, New Brunswick: Jour. Sed. Petrology, v. 44, p. 698-704.

Dingler, J. R., 1974, Wave-formed ripples in nearshore sands: Ph. D. Dissertation, Univ. California, San Diego, 136 p.

Harms, J. C., 1969, Hydraulic signifcance of some sand ripples: Geol. Soc. America Bull., v. 80, p. 363-396.

Homma, M. and Horikawa, K., 1975, Suspended Sediment due to Wave Action: Proc. 8th Coastal Eng., p. 168-193.

Inman, D. L., 1957, Wave-generated ripples in nearshore sands: U.S. Army Corps of Engineers, Beach Erosion Board Tech. Memo. 100, 66 p.

_____, and Bowen, A. J., 1963. Flume experiments on sand transport by waves and currents: AM. Soc. Civil Engineers, Proc. 8th Conf. on Coastal Eng., p. 137-150.

Jonsson, I. G., 1966, Wave Boundary Layers and Friction Factors: Proc. 10th Coastal Eng., Am. Soc. of Civil Engineers, p. 127-148.

Jonsson, I. G., 1975, Experimental and theoretical investigations in an oscillatory turbulent boundary layer: J. Hyd. Res., v. 14, no. 1, p. 45-59.

Kennedy, J. F. and Falcon, M., 1965, Wave generated sediment ripples: Report no. 86, Dept. Civil Eng., MIT, Cambridge, Mass.

Komar,P. D., 1974, Oscillatory ripple marks and the evaluation of ancient wave conditions and environments: Jour. Sed. Petrology, v. 44, p. 169-180.

_____ and Miller, M. C., 1973, The threshold of sediment movement under oscillatory water waves: Jour. Sed. Petrology, v. 43, p. 1101-1110.

_____ and _____, 1974, Sediment threshold under oscillatory waves: Am. Soc. Civil Engineers, Proc. 14th Conf. on Coastal Eng., p. 756-775.

Lofquist, K.E.B., Sand ripple growth in an oscillatory-flow water tunnel: U.S. Army Corps of Engrs., Coastal Eng. Res. Cent., Tech. Pap. 78-5.

Lyne, W. H., 1971, Unsteady viscous flow over a wavy wall: J. Fluid Mech., v. 50, no. 1, p. 33-48.

Madsen, O. S. and Grant, W. D., 1982, Movable bed roughness in unsteady oscillatory flow: Jour. Geophysical Res., v. 87, no. c1, p. 469-481.

_____ and _____, 1980, Combined wave and current interaction with a rough bottom: Jour. Geophysical Res. v. 84, no. c4, p. 1797-1808.

_____ and _____, 1975, The threshold of sediment movement under oscillatory waves: a discussion: Jour. Sed. Petrology, v. 45, no. 1, p. 359-367.

Manohar, V., 1955, Mechanics of bottom sediment movement due to wave action: TM-75, U.S. Army, Corps of Engineers, Beach Erosion Board, Washington, D.C.

Mogridge, G .R. and Kamphuis, J. W., 1972, Experiments on Bed Forms Generated by Wave Action: Proc. 13th Coastal Eng., p. 1123-1142.

Reineck, H. E., and Singh, I. B., 1973, Depositional sedimentary environments: Springer-Verlag, New York, 439 p.

Sleath, J. F. A., 1975, A contribution to the study of vortex ripples: J. Hyd. Res. v. 13, no.3, p. 315-328.

_____, 1974, Mass transport over a rough bed. J. Mar. Res., v. 32, no. 1, p. 13-24.

Southard, J. B., Harms, J. C., and Walker, R. G., 1982, Structures and Sequences in Clastic Rocks: Notes for Short Course No. 9, Soc. Economic Paleontologists and Mineralologists.

Southard, J. B., Boguchwal, L. A., and Romea R. D., 1980, Test of scale modelling of sediment transport in steady unidirestional flow: Earth Surface Processes, v. 5. p. 17-23.

Turnstall, E.B., 1973, Experimental Study of Vortices Generated by Oscillatory Flow Over Rippled Surfaces: Ph.D. Dissertation, Univ. of California, San Diego, 126 p.

Yalin, M. S. and Russell, R. C. H., 1962, Similarity in sediment transport due to waves: Proc. 8th Coastal Eng., p. 151-167.

LIST OF SYMBOLS

a	orbital radius
$2a$	orbital diameter
A	average bed height
D	sediment grain size
g	gravity
h	ripple height
Q	flow rate
T	period of oscillation
u	velocity fluctuation (x)
$\overline{U}$	average velocity
U_m	maximum orbital velocity
w	velocity fluctuation (z)
γ'	specific weight
η	fn. of Φ and δ
κ	von Karmann's constant
λ	ripple spacing
μ	viscosity
ν	kinematic viscosity
ρ	density of fluid
ρ_s	density of sand
ξ	mass transport distance
δ	boundary layer thickness
τ_m	boundary shear stress
Φ	velocity potential
ω	frequency in rads